JACS Au
AN OPEN ACCESS JOURNAL OF THE AMERICAN CHEMICAL SOCIETY

Editors' Choice
Open Access

pubs.acs.org/jacsau
Perspective

How Amorphous Nanomaterials Enhanced Electrocatalytic, SERS, and Mechanical Properties

Jianxin Kang,[#] Fengshi Li,[#] Ziyan Xu,[#] Xiangyu Chen, Mingke Sun, Yanhong Li, Xiuyi Yang,* and Lin Guo*

Cite This: *JACS Au* 2023, 3, 2660–2676

Read Online

ACCESS | Metrics & More | Article Recommendations

ABSTRACT: There is ever-growing research interest in nanomaterials because of the unique properties that emerge on the nanometer scale. While crystalline nanomaterials have received a surge of attention for exhibiting state-of-the-art properties in various fields, their amorphous counterparts have also attracted attention in recent years owing to their unique structural features that crystalline materials lack. In short, amorphous nanomaterials only have short-range order at the atomic scale, and their atomic packing lacks long-range periodic arrangement, in which the coordinatively unsaturated environment, isotropic atomic structure, and modulated electron state all contribute to their outstanding performance in various applications. Given their intriguing characteristics, we herein present a series of representative works to elaborate on the structural advantages of amorphous nanomaterials as well as their enhanced electrocatalytic, surface-enhanced Raman scattering (SERS), and mechanical properties, thereby elucidating the underlying structure−function relationship. We hope that this proposed relationship will be universally applicable, thus encouraging future work in the design of amorphous materials that show promising performance in a wide range of fields.

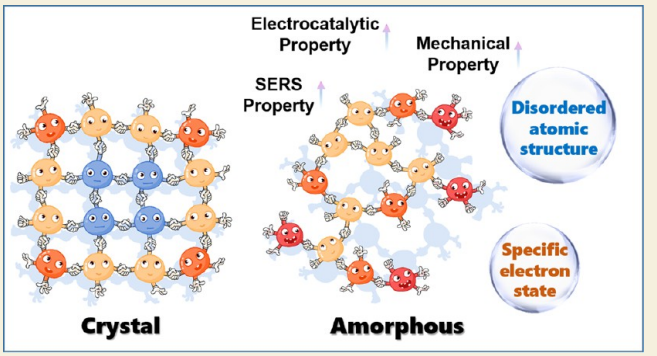

KEYWORDS: *Amorphous nanomaterials, Disordered atomic structure, Unsaturated coordination, Surficial dangling bond, Structural flexibility, Enhanced charge transfer*

1. INTRODUCTION

According to the definition of materials science, an amorphous material is a type of solid that lacks the long-range order characteristic of crystals and has only short-range order at the atomic length scale due to unique intermolecular chemical bonding. The definition of amorphous materials is derived from their crystalline counterparts, leading to their delayed development. In crystals, the ordered atomic arrangement and regular morphology greatly simplify the process of experimental observation and theoretical analysis of the materials.[1−3] Due to advanced knowledge and techniques from other disciplines, such as point groups and space groups based on mathematics, and X-ray diffraction based on physics, crystallography has gradually become a mature and comprehensive subject.[4] However, this is not the case for amorphous materials, as they only retain the chemical unit over a short-range, which makes experimental characterization more challenging.[5,6] Of note, since the atomic arrangements in the amorphous materials are not constrained by fundamental atomic groups, the specific positions and orientations of atomic groups remain elusive. Amorphous materials are still in their infancy, and extensively studied empirical laws are still urgently required to gain an in-depth understanding of the novel properties of these materials.

Amorphous nanomaterials combine the unique features of nanostructures and amorphous structures, which can bring many interesting properties and are considered to be a greatly significant research direction.[7−9] Compared with traditional nanomaterials with large specific surface area, amorphous nanomaterials with disordered atomic structure could further improve the exposed surface, resulting in a high concentration of surficial active sites, which provides a new perspective for exhibiting the intrinsic properties of materials.[10−12] In addition to pure amorphous nanomaterials, some partially amorphous nanomaterials also deserve close study.[13] Typically, in reduced-size crystalline nanomaterials, surface relaxation and interfacial effects can alter the position of certain atoms on the surface, thus

Received: July 28, 2023
Revised: September 18, 2023
Accepted: September 20, 2023
Published: October 8, 2023

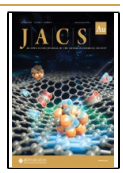

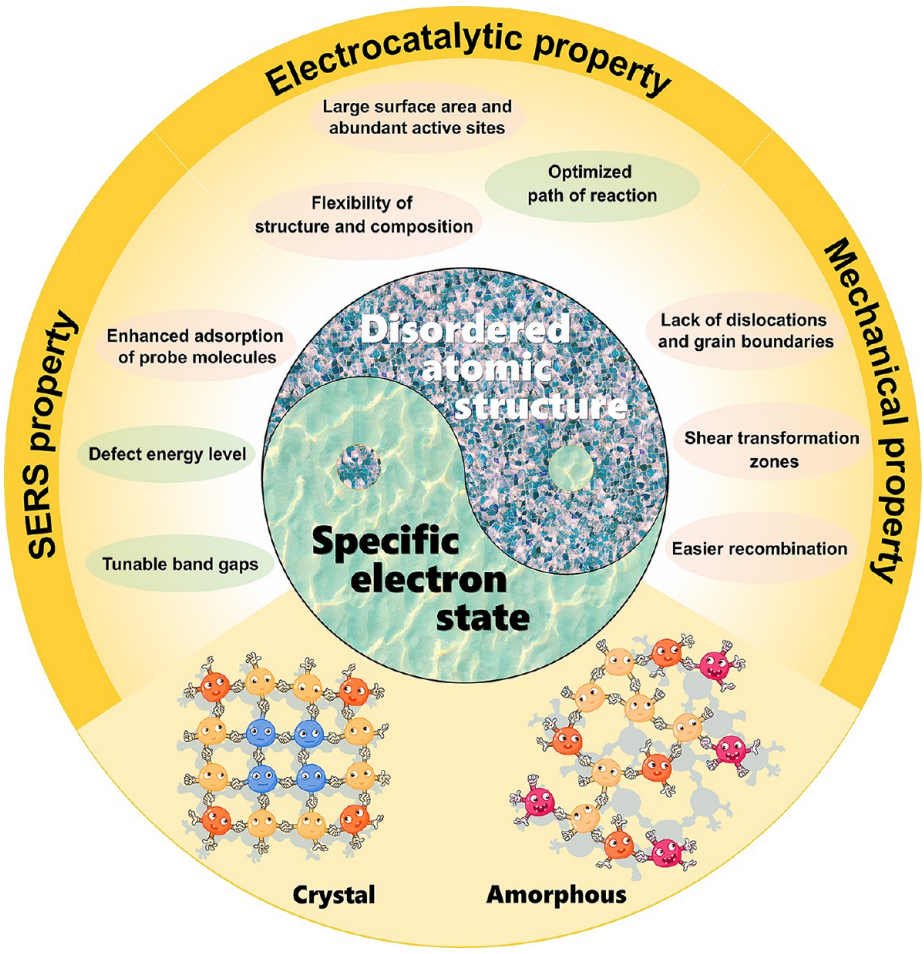

Figure 1. Schematic illustration of the unique structural features of amorphous nanomaterials in electrocatalytic, SERS, and mechanical aspects.

affecting the structural order and creating amorphous shells or amorphous domains. This partially amorphous structure also shows the particular advantages of enhanced performance due to a particular disordered atomic arrangement and interfacial microstructure. Apart from this, it has been determined by *Ostwald's rule* that the amorphous solid phase has a high solubility and is always the first to precipitate out of solution,[14,15] which endows amorphous nanomaterials with an irreplaceable role in deepening the principles of solid growth in liquids.[16,17] In this regard, unraveling the relationship between the amorphous structures and their specific properties is also of great significance for the development of crystalline materials.

Amorphous nanomaterials possess unique structural features that crystalline materials lack, which may lead to their distinct electrocatalytic, surface-enhanced Raman scattering (SERS), and mechanical properties. The performance of these three areas shares many general relationships with the specific structures of amorphous nanomaterials (Figure 1). For example, the coordinatively unsaturated surface produces more active sites in electrocatalysis which enhances the catalytic performance. At the same time, it also makes it easier for amorphous substrates to bind the adsorbed molecules and form surface complexes in the SRES effect. In addition, the coordinatively unsaturated surface also makes it easier for amorphous nanomaterials to recombine with other surrounding units, forming new superstrong interfacial interactions in mechanical performance. In addition to a specific atomic structure, the specific electron states of the amorphous nanomaterial can optimize the reaction pathways and enhance the intrinsic activity of electrocatalytic active sites. It can also realize tunable energy levels and facilitate charge transfer process in the SRES effect. Therefore, a unified discussion in different fields may lead to new directions for further tuning the properties of amorphous nanomaterials and create exciting research fields. In this Perspective, we first summarize the plentiful active sites and flexible structure induced by the long-range disordered atomic structure of amorphous nanomaterials to promote electrochemical activity.[18−21] Then, the modulated electronic state of amorphous nanomaterials (band structure of amorphous semiconductor substrate, charge transfer pathway and vibrational coupling of probe molecules, *etc.*) are elucidated to enhance Raman signal of absorbed molecules.[22−24] We also present the intrinsic mechanical properties of amorphous nanomaterials in terms of their atomic isotropic characteristics, where unsaturated dangling bonds stimulate superstrong interfacial interactions with other surrounding components.[25−27] Finally, challenges and suggestions for future research on amorphous nanomaterials are also provided. We hope that the initial elucidation of the structure−function relationship of amorphous nanomaterials will encourage the future design of applicable amorphous nanomaterials that exhibit promising performance in a wide range of fields.

https://doi.org/10.1021/jacsau.3c00418
JACS Au 2023, 3, 2660−2676

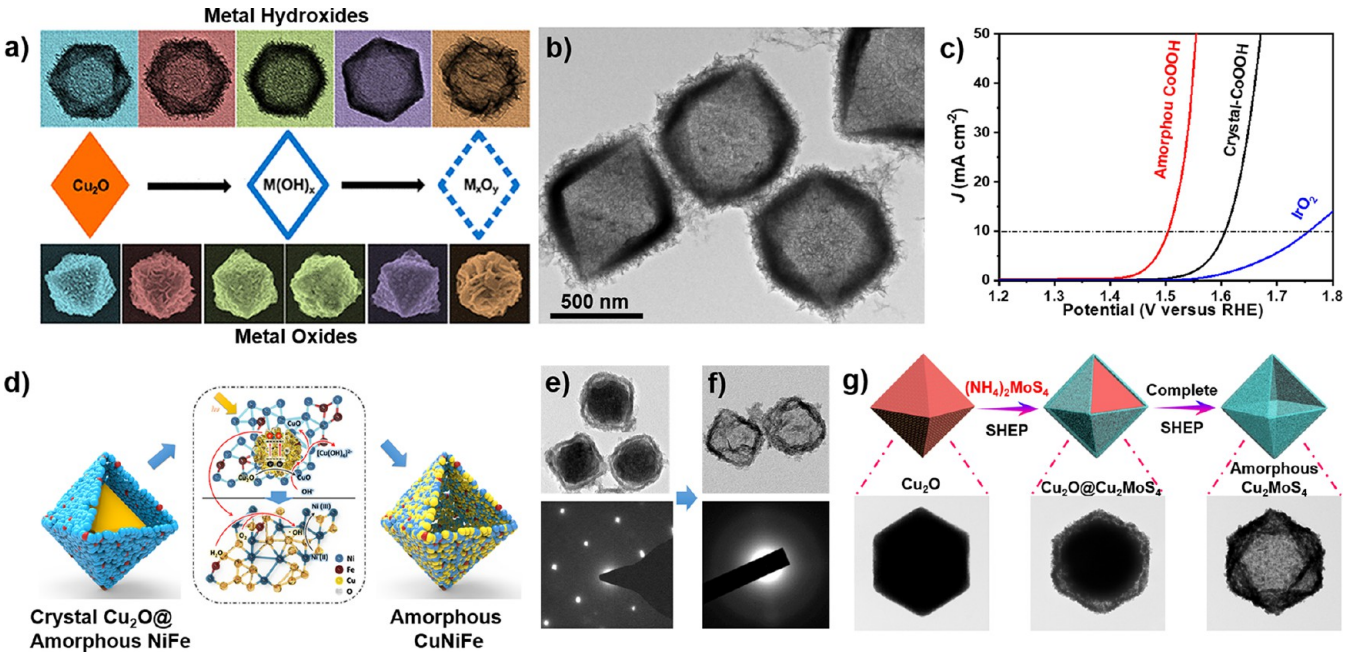

Figure 2. Morphology and electrocatalytic performance of different amorphous nanocages. (a) Morphology of different amorphous metal hydroxide nanocages (from left to right: Mn, Fe, Co, Ni, Zn) and corresponding metal oxides. (b, c) Transmission electron microscopy (TEM) image and OER performance of amorphous $Co(OH)_2$ nanocages. (d) Schematic diagram of the photocorrosion engineering strategy and the OER enhancement mechanism of amorphous CuNiFe hydroxide nanocage. (e, f) TEM images (top panels) and selected area electron diffraction (SAED) patterns (bottom panels) of the amorphous CuNiFe sample before and after photocorrosion. (g) Formation process of ternary amorphous nanocages by the SHEP method. Panel (a) is adapted with permission from ref 30. Copyright 2013 American Chemical Society. Panels (b, c) are adapted with permission from ref 19. Copyright 2018 WILEY-VCH Verlag GmbH & Co. KGaA, Weinheim. Panels (d–f) are adapted with permission from ref 33. Copyright 2019 Wiley-VCH Verlag GmbH & Co. KGaA, Weinheim. Panel (g) is adapted with permission from ref 34. Copyright 2019 Science China Press and Springer-Verlag GmbH Germany, part of Springer Nature.

2. AMORPHOUS MATERIALS IN ENHANCED ELECTROCATALYSIS

The development of sustainable and clean energy sources such as solar, wind, and hydrogen to meet the huge energy demands of the future is gaining momentum. In recent years, particular attention has been paid to the development of electrochemical energy conversion and storage devices to balance power generation and consumption and effectively store energy for future use. In enhancing the efficiency of energy conversion devices, the atomic and electronic structures of the electrocatalysts play the key role in governing the electrochemical kinetics. It has been reported in full that there are two strategies to improve the activity of a given catalyst.[28] One strategy is to increase the number of active sites by optimizing the particular surface area and the degree of unsaturated coordination. The other strategy is to adjust the atomic structure and electron state to enhance the activity of each active site. In view of this, amorphous nanomaterials are proposed to further enhance the electrocatalytic performance of crystalline nanomaterials with simultaneously increased number and activity of reaction sites. Thus, amorphous nanomaterials exhibiting hollow or low-dimensional morphologies are recommended. Apart from this, the amorphous structure possesses abundant active sites and a unique electron structure, which confers a new and superior performance upon some traditional crystalline materials, resulting in a new class of highly efficient electrocatalytic systems.

2.1. Amorphous Hollow Nanocages in Electrocatalysis

Inspired by Pearson's hard and soft acid–base principle, a general strategy was proposed to synthesize well-defined hydroxide three-dimensional (3D) nanocages with controllable components, shell thickness, shape, and size through a coordination etching strategy at room temperature (Figure 2a).[29,30] As a typical example, amorphous $Co(OH)_2$ nanocages showed a low overpotential of 0.28 V at 10 mA cm^{-2} in the oxygen evolution reaction (OER), which proves much better than their crystalline counterparts (Figure 2b, c).[19] The enhanced activity can be attributed to the high structural flexibility of the amorphous structure concentrated on the following three aspects. First, amorphous $Co(OH)_2$ showed a more negative potential and a larger current during the electrochemical conversion into CoOOH, highlighting its excellent ability to transform into a catalytic active phase as a whole. Second, amorphous $Co(OH)_2$ possessed a higher concentration of oxygen vacancies, which is favorable for OER. Lastly, amorphous $Co(OH)_2$ demonstrated better self-regulation behaviors, as it underwent reconfiguration and optimization of its coordination structure during electrocatalysis. Therefore, this pioneering work serves as a desirable platform for researchers to further their understanding of the underlying mechanisms when amorphous materials are used in electrocatalysis.

To explore the synergistic effect between multimetal elements, this method was further extended to synthesize amorphous Ni–Co and Ni–Zn double hydroxide nanocages.[31,32] With the unique amorphous hollow nanostructure, their OER performance could reach a high level by exhibiting a very low overpotential (0.25 V for Ni–Co at a current density of 10 mA cm^{-2}) and high mass activity (285.6 A g^{-1} for Ni–Zn at an overpotential of 0.3 V). For more complicated trimetallic hydroxide compounds, a novel photocorrosion engineering

https://doi.org/10.1021/jacsau.3c00418
JACS Au 2023, 3, 2660–2676

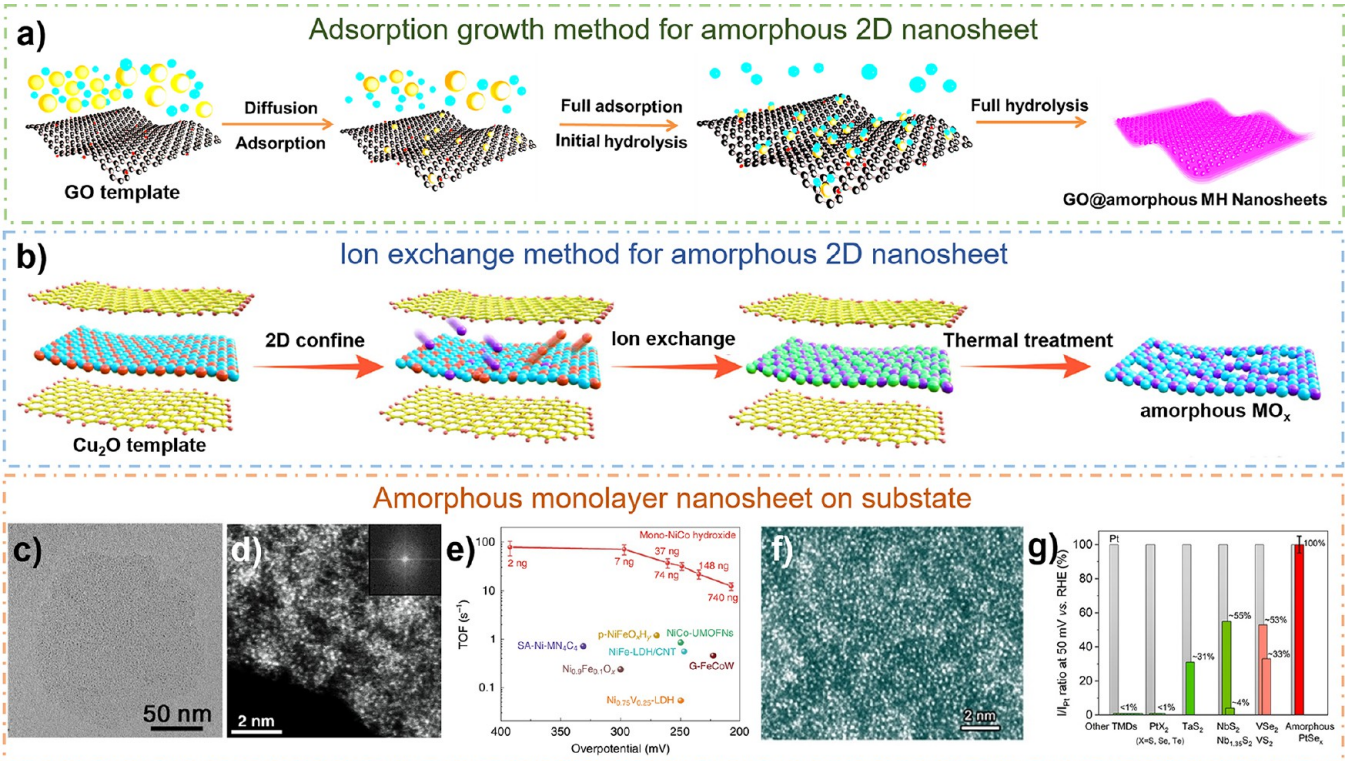

Figure 3. Growth mechanism, morphology, and electrocatalytic performance of different amorphous nanosheets. (a, b) Schematic diagrams of the adsorption growth method and ion exchange method for the synthesis of amorphous nanosheets. (c) TEM image of monolayer $Ni(acac)_2$. (d, e) High-angle annular dark field (HAADF) image and TOF comparison of amorphous monolayer $Ni(OH)_2$. (f) HAADF image of amorphous $PtSe_x$ film. (g) Current density ratios of amorphous $PtSe_x$ film and related transition metal dichalcogenide based catalysts with respect to the Pt catalyst. Panel (a) is adapted with permission from ref 35. Copyright 2017 Wiley-VCH Verlag GmbH & Co. KGaA, Weinheim. Panel (b) is adapted with permission from ref 37. Copyright 2020 American Chemical Society. Panels (c, e) are adapted with permission from ref 21. Copyright 2021 Springer Nature. Panel (d) is adapted with permission from ref 40. Copyright 2022 American Chemical Society. Panels (f, g) are adapted with permission from ref 39. Copyright 2022 Springer Nature.

strategy was developed by introducing additional metal elements into the as-constructed amorphous nanocages (Figure 2d).[33] The prepared amorphous ternary Cu−Ni−Fe hydro(oxy)oxide nanocages (Figure 2e, f) exhibited the highest reported mass activity of over 1400 A g^{-1} at an overpotential of 0.3 V in the OER (Figure 2g). Herein, the amorphous structure, the synergistic effect between the multiple elements as well as the optimized 3d electronic structure and the adsorption energy of the OER intermediates are the main factors that greatly improve the electrocatalytic performance. In addition to hydroxides, metal sulfides have also been synthesized in the form of amorphous nanocages by the controllable self-hydrolyzing etching-precipitating (SHEP) method, demonstrating the universality of this strategy.[34] The as-made hollow amorphous Cu_2MoS_4 nanocage with plenty of sulfur vacancies endows it with a superior hydrogen evolution reaction (HER) performance.

2.2. Amorphous Nanosheets in Electrocatalysis

Apart from the hollow structure, the ultrathin amorphous 2D nanosheet with rich exposed atoms on the surface is another alternative structure for catalysts. A range of universal strategies have been developed for the controllable synthesis of ultrathin amorphous nanomaterials, ranging from hydroxides to oxides with mono-, binary- and ternary-elements (Figure 3a, b).[35−37] An ultrathin, amorphous Co−V hydr(oxy)oxide nanosheet with a thickness of ∼0.7 nm was synthesized. It exhibited a remarkably low overpotential of 250 mV at 10 mA cm^{-2} in OER, which was the best among its counterparts.[20] Unlike its crystalline counterpart, the amorphous product could easily transform from its original phase to the real active phase with preferred active Co valence states. Meanwhile, the flexibility of the amorphous structure ensured long-term stability, with a stable operating time of 170 h in an alkaline medium. Besides the liquid phase synthesis method, a general solid phase approach has also been demonstrated to synthesize a series of noble metal amorphous nanosheets such as monometallic nanosheets (Ir, Rh, Ru), bimetallic nanosheets (RhFe, IrRu) and trimetallic nanosheets (IrRhRu) by annealing the mixture of metal acetylacetonate and alkali salts.[38] Taking Ir-based amorphous nanosheets as an example, they have abundant active sites and a faster charge transfer process, demonstrating a superior catalytic performance than the conventional corresponding crystalline catalysts, with mass activity increased by 2.5 times.

With this in mind, we focused on the catalytic performance of monolayer amorphous nanosheets. Through *in situ* electrochemical conversion, monolayer molecular crystals of $Ni(acac)_2$ were used as precursors to construct amorphous monolayer $Ni(OH)_2$ on the electrode (Figure 3c, d). By taking advantage of the repulsive force between the methyl groups on the surface of $Ni(acac)_2$, possible stacking during the formation and storage of the monolayers could be avoided.[21] The monolayer feature facilitated the dehydrogenation of $Ni(OH)_2$ and accelerated its transformation into the active phase with higher valence states of Ni. Coupled with the doping of Co, it was found that the release of lattice oxygen in the monolayer amorphous NiCo hydroxides

https://doi.org/10.1021/jacsau.3c00418
JACS Au 2023, 3, 2660−2676

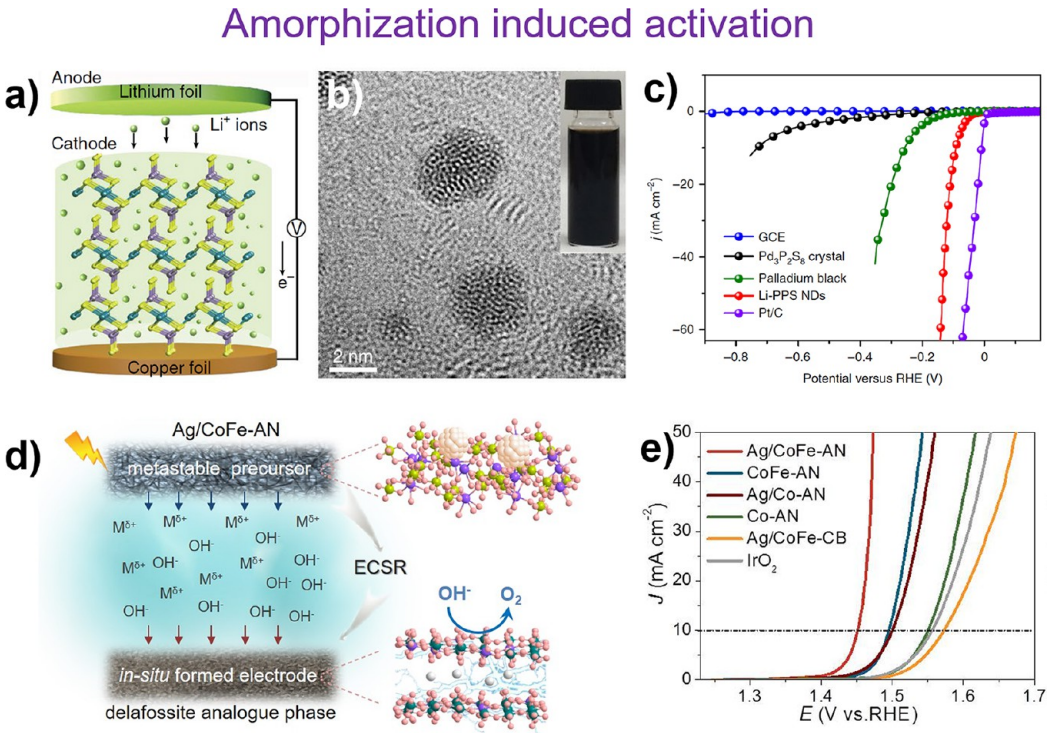

Figure 4. Amorphization-induced activation in electrocatalysis. (a) Schematic diagram of the conversion from layered $Pd_3P_2S_8$ to amorphous lithium-incorporated palladium phosphosulfide nanodots. (b, c) TEM image and HER performance of the amorphous lithium-incorporated palladium phosphosulfide nanodots. (d) Schematic diagram of the self-reconstruction process for the preparation of the delafossite analog. (e) OER performance of the as-prepared delafossite analogs. Panels (a−c) are adapted with permission from ref 45. Copyright 2018 Springer Nature. Panels (d, e) are adapted with permission from ref 18. Copyright 2020 National Academy of Sciences.

was accelerated. This was because Co^{3+} in the Jahn−Teller distortion field of Ni^{3+} exhibited a high-spin crystal field structure with two long axes and four short axes, allowing it to readily capture electrons at relatively lower valence electron energy levels and produce oxygen vacancies. The generated large number of coordinatively unsaturated metal sites were considered to be the real active sites for water oxidation, which significantly reduced the overpotential and enhanced the catalytic efficiency. Taking advantage of the amorphous atomic structure and monolayer feature, the catalyst displayed superior OER activity with a remarkably high turnover frequency (TOF) of ∼10−70 s^{-1}, orders of magnitude higher than that of the best catalyst ever reported (Figure 3e). The facilitated dehydrogenation of monolayer amorphous $Ni(OH)_2$ has also been applied to energy storage, yielding almost twice the theoretical capacity of bulk $Ni(OH)_2$.[40] Compared to bulk $Ni(OH)_2$ which transfers only one electron in charge−discharge cycles, monolayer amorphous $Ni(OH)_2$ exhibited two discharge processes with two electron transfers, demonstrating a more efficient energy storage mechanism. The construction of an amorphous monolayer on a substate directly used as an electrode is a promising direction to further enhance the performance of certain materials. For example, a wafer-size amorphous monolayer $PtSe_x$ film has been constructed on a SiO_2 substate that processes a maximum density of active sites enabled by the amorphous structure (Figure 3f).[39] With a fully activated surface, it exhibits a current density of almost 100% relative to that of a pure Pt surface in HER and is close to the best among current transition metal dichalcogenide catalysts (Figure 3g).

2.3. Amorphization Induced Revitalization for in Electrocatalysis

In addition to the direct synthesis of amorphous nanomaterials to promote the existing electrocatalytic activity of crystalline counterparts, the *in situ* self-reconstruction of amorphous species produced from the crystal during catalysis has been found to be a key to electrocatalysis.[41] It is widely believed that, even for a crystal catalyst, the reconstructed amorphous structure is considered to be the real active phase that is advantageous to the catalytic process.[42−44] Thus, amorphization could also bring new properties to inactive traditional crystal materials. For example, unlike the layered hydroxides, which are well-known to be excellent active materials for the OER, some lamellar materials show poor intrinsic activity and electronic conductivity, resulting in inferior catalytic performance. Encouragingly, it has been reported that amorphization has been confirmed as a powerful and compelling strategy to engineer material structures at the atomic level and to revitalize the catalytic activity. A major breakthrough has been achieved in promoting the performance of ternary palladium thiophosphate ($Pd_3P_2S_8$) with a layered structure, although its inconspicuous properties have led to few reports of its exploration for any applications. An electrochemical lithiation process was skillfully employed to realize the amorphization of layered $Pd_3P_2S_8$ crystal (Figure 4a).[45] The produced amorphous lithium-incorporated palladium phosphosulfide nanodots with abundant vacancies exhibited excellent electrocatalytic activity and outstanding long-term stability for HER (Figure 4b, c). Similar to layered $Pd_3P_2S_8$, the delafossites (ABO_2) constructed by two-dimensional (2D) layers of edge-linked BO_2 octahedra were usually inactive for electrocatalysis. In order to subvert the status quo, a

https://doi.org/10.1021/jacsau.3c00418
JACS Au 2023, 3, 2660−2676

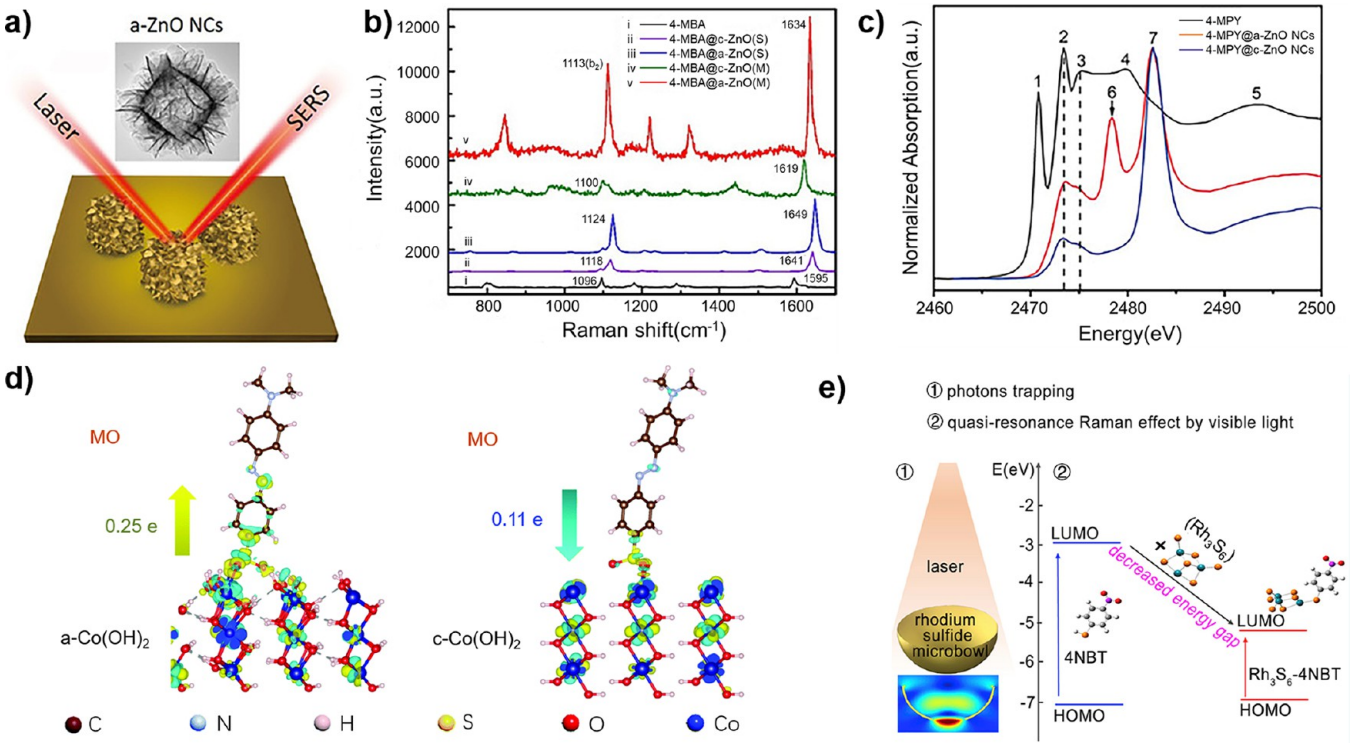

Figure 5. Enhanced adsorption of molecules in amorphous semiconductor materials. (a) Schematic diagram of the use of amorphous ZnO nanocages as a SERS substrate; (b) Measured and simulated SERS spectra of 4-MBA molecules (10^{-4} M) adsorbed onto c- and a-ZnO NCs; (c) Sulfur K-edge XANES spectra of pure 4-MPY molecules and 4-MPY adsorbed on c- and a-ZnO NCs; (d) Charge difference distributions for MO adsorbed on amorphous $Co(OH)_2$ and crystalline $Co(OH)_2$. (e) SERS activity observed from amorphous rhodium sulfide microbowl substrates. Panels (a–c) are adapted with permission from ref 60. Copyright 2017 Wiley-VCH Verlag GmbH & Co. KGaA, Weinheim. Panel (d) is adapted with permission from ref 59. Copyright 2022 Royal Society of Chemistry. Panel (e) is adapted with permission from ref 23. Copyright 2018 The Author(s).

delafossite analog ($AgCoO_2$) with an amorphous structure was synthesized by the conversion of metal oxyhydroxide and delafossite (Figure 4d).[18] The resulting geometric structure with finely tuned local electronic states provided amorphous $AgCoO_2$ with a superior OER performance. Since Ag atoms were larger than H atoms, the specific axial directions in the Co−O_6 crystal field were thought to be elongated, which was attributed to the competition between hydrogen bonding and the spatial occupancy effect of Ag. The unevenly distributed local stress in the amorphous material, which produced the high-spin state of Co^{3+}, promoted the activity of the Co sites. The enhanced intrinsic activity, reduced activation energy, increased accessible active sites and enhanced electrical conductivity resulted in an even lower overpotential of 220 mV (10 mA cm^{-2}) and excellent electrochemical durability in OER (Figure 4e). The amorphization treatment provides a new opportunity for the future development of the potential of traditional crystal materials. It goes without saying that a thorough understanding of the mechanism, such as the structure−function relationship, will further broaden their applications.

Overall, the amorphous nanomaterials, whether the above-mentioned 3D nanocages and 2D nanosheets or lower dimensional nanowires,[46] nanorods,[47] nanoparticles[48,49] or clusters,[50] have been widely reported to significantly enhance the electrocatalytic performance. Based on these representative works, amorphous nanomaterials offer a new and potent way to further promote the electrocatalytic performance of their crystalline counterparts through the following pathways:

1. Coordinatively unsaturated structures of amorphous nanomaterials improve the large specific surface area of traditional nanomaterials to high concentration of surface active sites, enhancing the overall catalytic activity.[33,48]
2. The long-range disordered nature of amorphous nanomaterials endows them with structural flexibility, allowing self-regulation and even self-repair under electrocatalytic conditions, providing long-term stability of the catalyst. Amorphous nanomaterials could also provide the flexibility of chemical composition, resulting in substoichiometric atomic ratios to explore more effective or selective catalysts than their crystalline counterparts.[19,20,31,50]
3. The unique structure of amorphous nanomaterials modulates the electron states, optimizing the multistep reaction pathway and enhancing the intrinsic activity of active sites.[18,21]

3. AMORPHOUS MATERIALS IN ENHANCED SERS PROPERTY

In recent years, amorphous semiconductor materials have gained widespread popularity because of their impressive optical properties in a variety of areas, including light absorption, light scattering, surface charge transfer, luminescence, *etc.* In essence, the optical properties of matter are the macroscopic manifestation of the interaction between photons and electrons/phonons. The unique optical properties of amorphous semiconductor materials arise from their special electronic and energy band structures, which are different from those of crystals. As a matter of fact, people are more familiar with crystalline semiconductors, whose electron wave function can be represented by the Bloch function to describe

https://doi.org/10.1021/jacsau.3c00418
JACS Au 2023, 3, 2660−2676

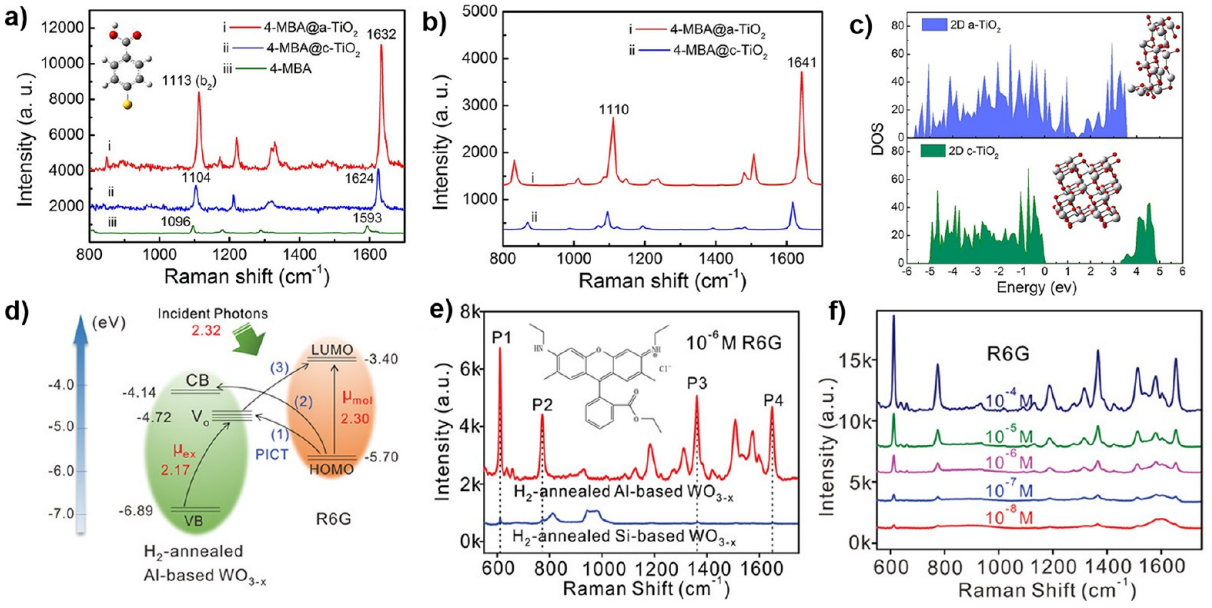

Figure 6. Tunable band gaps and energy levels of amorphous semiconductors. (a) SERS spectra of 4-MBA (10^{-4} M) molecules adsorbed on c- and a-TiO_2 NSs and the normal Raman spectrum of pure 4-MBA solution (0.1 M). (b) Simulated SERS spectra of 4-MBA @a-TiO_2 NSs and 4-MBA @c-TiO_2 NSs. (c) DOS calculation of c- and a-TiO_2 NSs. (d) Energy level diagram of R6G molecule adsorbed on the amorphous WO_{3-x} SERS substrates. (e) SERS spectra of R6G molecules (10^{-6} M) absorbed on crystalline and amorphous WO_{3-x} films. (f) SERS spectra of different concentrations of R6G molecules adsorbed on amorphous WO_{3-x} films. Panels (a–c) are adapted with permission from ref 22. Copyright 2019 American Chemical Society. Panels (d–f) are adapted with permission from ref 24. Copyright 2019 WILEY-VCH Verlag GmbH & Co. KGaA, Weinheim.

the coopted motion of the electrons. In contrast, the long-range disordered atomic arrangement of amorphous semiconductors makes their electronic states no longer restricted to the extended ones. Moreover, both the conduction and valence bands of amorphous semiconductors have band tails that extend into the forbidden band. Therefore, the bottom of the conduction band and the top of the valence band are filled with fuzzy band tails. These properties result in amorphous semiconductors with significantly different optical properties from those of crystalline semiconductors.

The SERS effect refers to a phenomenon in which the Raman signal of molecules adsorbed on certain substrate surfaces is greatly enhanced, which can increase the intensity of the conventional Raman signal by a factor of 10^2 to 10^{14} and extend the lowest detection limit of typical molecules to the single molecule level.[51,52] Two mechanisms can be used to explain this significant enhancement of the Raman signal: one is the electromagnetic enhancement (EM) mechanism based on the localized surface plasmon resonance (LSPR) effect of noble metal nanostructures,[53] and the other is the chemical enhancement (CM) mechanism based on the charge transfer (CT) between the substrate and the adsorbed molecules.[54] It is well-known that, with the exception of a few semiconducting materials (e.g., molybdenum oxides[55,56]), the free electron density of most semiconductors is insufficient to support the surface plasmon resonance effect in the visible region. Therefore, the SERS enhancement of semiconductor materials generally comes from chemical enhancement,[57] i.e., the formation of molecule–substrate surface complexes and the CT between molecules and substrates. In other words, one of the most important ways to enhance the SERS performance of semiconductor substrates is to increase the CT between the substrate and the molecule. In crystalline semiconductor materials, the periodic structure of the lattice enhances the constraint on the electrons, whereas on the surface of amorphous semiconductors, there are a large number of dangling bonds, causing the energy of the system to enter a metastable state. Therefore, compared to crystalline semiconductors, the binding of amorphous semiconductors to adsorbed molecules is stronger and the surface CT to adsorbed molecules is improved.[23,58−60] In addition, in terms of energy level tuning, amorphous semiconductors can provide tunable band gap and defect state energy levels,[23,61] which allows better energy level matching with the analyte molecule, thus resulting in stronger CT. Such a significant improvement in CT would result in a significant enhancement of the Raman signal of the adsorbed molecules in the system.

3.1. Enhanced Adsorption of Molecules

The abundance of unsaturated adsorption sites on the surface makes it easier for amorphous semiconductors to combine with adsorbed molecules to form surface complexes, coupled with the metastable electronic state of the amorphous state, which greatly improves the CT efficiency. To better utilize the unsaturated adsorption sites on the surface, amorphous ZnO nanocages (a-ZnO NCs) consisting of ultrathin amorphous ZnO nanosheets were designed, which presented ultrahigh SERS activity of 4-mercaptobenzoic acid (4-MBA) with an enhancement factor (EF) of up to 6.62×10^5 (Figure 5a, b).[60] This remarkable sensitivity could be attributed to the highly efficient CT between the substrate and the molecule. Compared to crystalline ZnO NCs, the metastable electronic states of the amorphous ZnO NCs exhibited a weaker constraint on the surface electrons, resulting in efficient interfacial CT. Furthermore, the efficient CT enabled a-ZnO NCs to form Zn–S π bonds with adsorbed 4-Mercaptopyridine (4-MPY), as demonstrated by X-ray absorption near-edge structure (XANES) characterization (Figure 5c). This is the first time that such high SERS activity has been observed on amorphous semiconductor substrates. In addition to metal oxides, amorphous metal hydroxide nanocages

https://doi.org/10.1021/jacsau.3c00418
JACS Au 2023, 3, 2660−2676

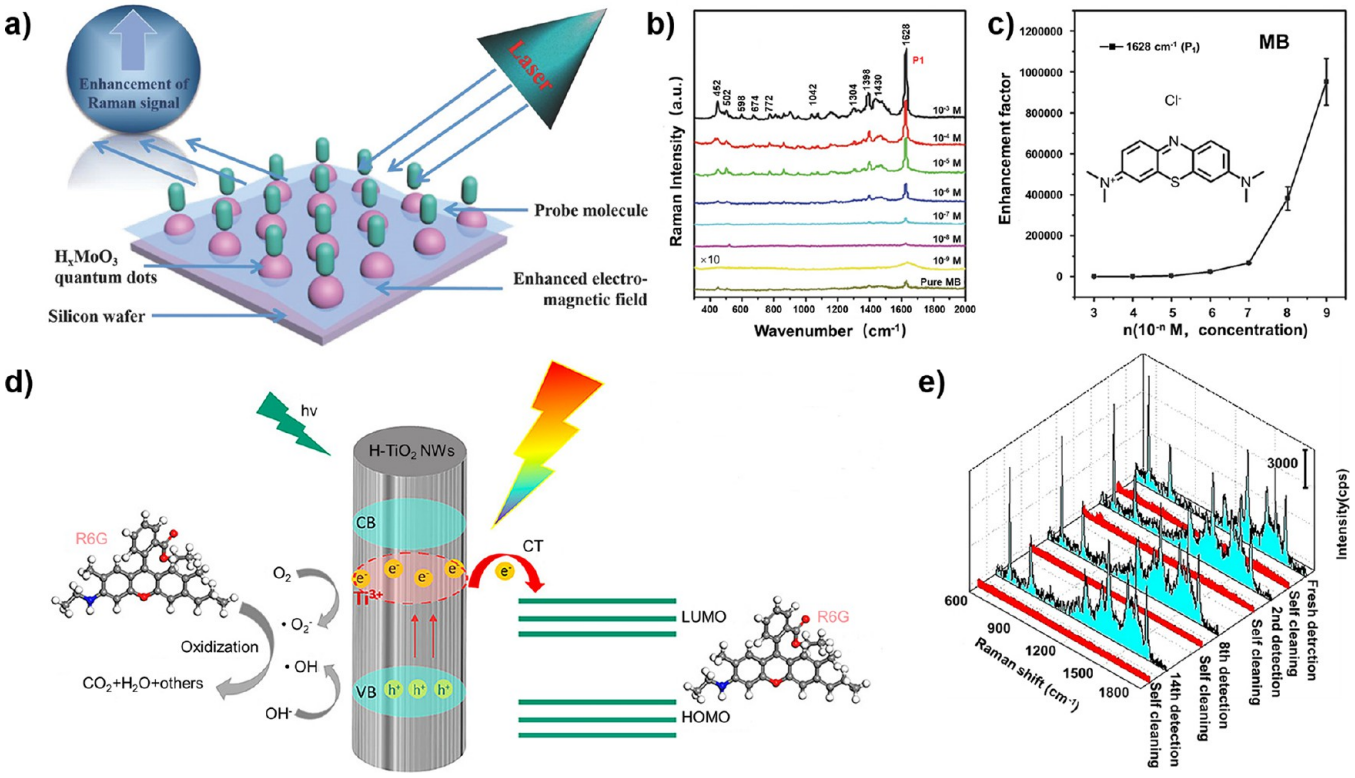

Figure 7. Tunable plasmon resonance effect of amorphous semiconductors. (a) Schematic diagram of the used of amorphous H_xMoO_3 quantum dots as a SERS substrate. (b) SERS spectra collected from seven different concentrations of MB molecule (10^{-3} to 10^{-9} M) on H_xMoO_3 substrates and the normal Raman spectrum of pure MB (10^{-2} M). (c) Relationship between the EF of H_xMoO_3 substrates and the concentration of MB molecules. (d) Hydrogenated black TiO_2 nanowires with high SERS activity and photodegradation capability. (e) SERS spectra of R6G adsorbed on hydrogenated TiO_2 substrate recorded over 14 cycles of recycling. Each cycle consists of absorption and degradation of 1×10^{-6} M R6G on hydrogenated TiO_2 substrate and recording of SERS spectra of R6G on hydrogenated TiO_2 substrate before and after UV light irradiation. Panels (a–c) are adapted with permission from ref 64. Copyright 2018 WILEY-VCH Verlag GmbH & Co. KGaA, Weinheim. Panels (d, e) are adapted with permission from ref 65. Copyright 2018 American Chemical Society.

have also been explored.[59] For example, compared with the crystalline counterparts, the surface of amorphous $Co(OH)_2$ exhibited a low coordination number of Co atoms and a large number of oxygen defects. Therefore, it was easier to form Co–O bonds and strong hydrogen bonds between amorphous $Co(OH)_2$ and methyl orange (MO), which promoted the formation of stable surface CT complexes and CT between the substrates and the adsorbed molecules. The density functional theory (DFT) simulations showed that the amorphous $Co(OH)_2$ allowed a larger number of charges to be transferred between the $Co(OH)_2$ surface and the MO molecules compared to that of the crystalline $Co(OH)_2$ (Figure 5d). Finally, an enhancement factor of $1.56 \times 1 \times 10^5$ was achieved for the MO molecule. To further obtain enrichment at a higher concentration, amorphous rhodium sulfide microbowls were also designed, which exhibit remarkable SERS sensitivity with a high EF of 1×10^5 for rhodamine 6G (R6G).[23] The 4-nitrobenzenethiol (4NBT) molecule could also be adsorbed on amorphous Rh_3S_6 through Rh–S bonds. The polarizabilities and charge difference distributions of the Rh_3S_6-4NBT complex were calculated, and the results showed that the Rh–S bond could act as a CT channel, causing the deformation of the electron cloud of the 4-NBT molecule, amplifying the molecular polarizability and finally resulting in a highly enhanced Raman signal of 4NBT (Figure 5e).

3.2. Tunable Band Gaps and Energy Levels

Amorphous semiconductor materials also possess tunable band gaps and energy levels, which make it easier to achieve an energy level matching with adsorbed molecules and excited light, leading to stronger CT. The 2D amorphous TiO_2 nanosheets (a-TiO_2 NSs), could achieve an ultrahigh EF of 1.86×10^6 using 4-mercaptobenzoic acid (4-MBA) as a probe molecule (Figure 6a).[22] And the experimental results were in good agreement with the simulation results (Figure 6b). The DFT calculations showed that 2D a-TiO_2 possessed a smaller band gap and a higher density of states (DOS) compared to its crystalline counterpart (Figure 6c). Therefore, stronger energy-level coupling and CT could be observed between amorphous TiO_2 and adsorbed 4-MBA molecules. By calculating the charge difference distribution of 4-MBA@ crystalline and amorphous TiO_2, the Hirshfeld population analysis indicated that a great amount of charge was transferred from the 4-MBA molecules to the a-TiO_2. Similarly, amorphous TiO_2 aerogels enriched with oxygen vacancies on the surface also exhibited excellent SERS performance, which was attributed to the tuning of the energy band structure, resulting in the CT efficiency.[61] In addition, it was found that the combination of amorphous and non-stoichiometric features in amorphous WO_{3-x} films resulted in a narrower band gap, stronger exciton resonances and higher DOS near the Fermi energy level.[24] These properties facilitated the CT effect and enhanced the vibrational coupling between the substrate and the adsorbed molecules (Figure 6d). Ultimately,

https://doi.org/10.1021/jacsau.3c00418
JACS Au 2023, 3, 2660–2676

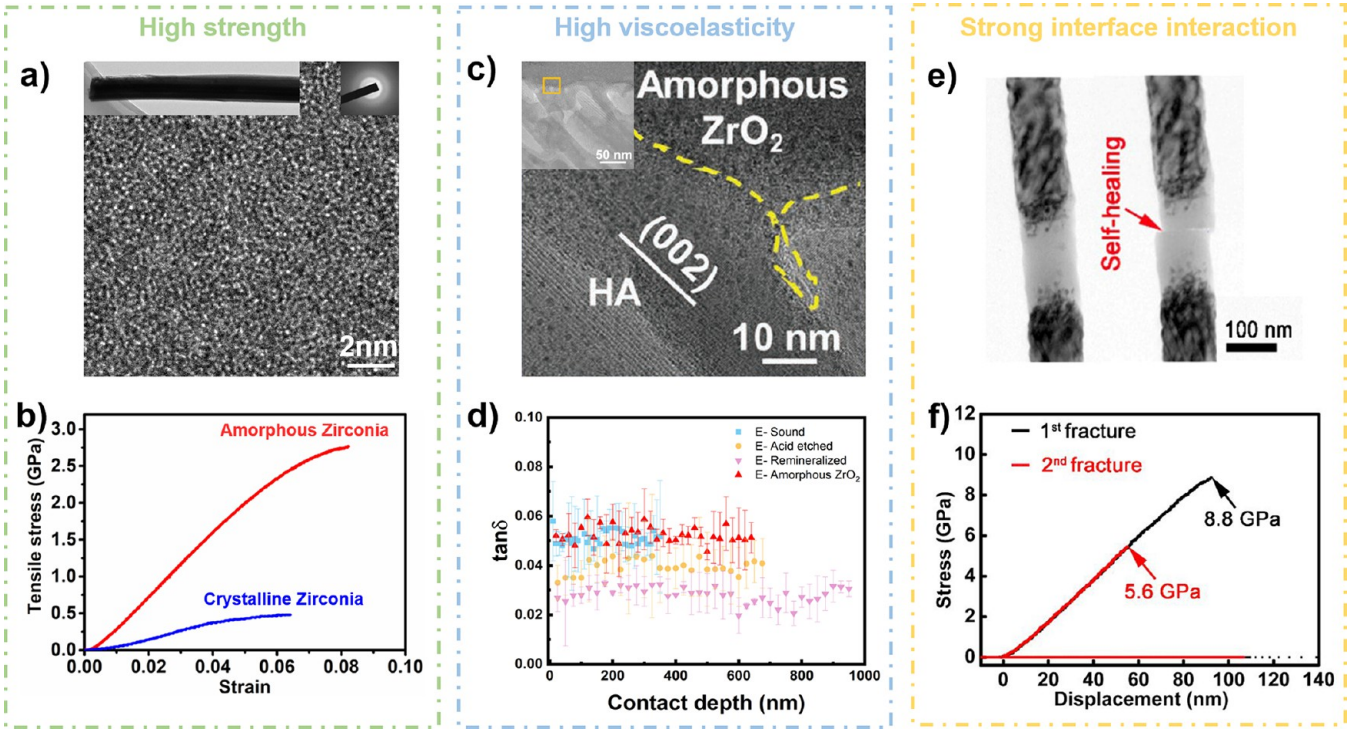

Figure 8. Mechanical properties of amorphous nanomaterials. (a) TEM images and SAED pattern of the amorphous ZrO_2 nanowire. (b) Stress−strain curves of the amorphous and crystalline zirconia nanowires. (c) TEM images of the enamel covered by the amorphous ZrO_2. (d) Damping coefficient of different enamels. (e) TEM images of amorphous SiC before fracture and self-healing. (f) Stress-displacement curves of SiC nanowire at the first and second fracture. Panels (a and b) are adapted with permission from ref 73. Copyright 2019 American Chemical Society. Panels (c and d) are adapted with permission from ref 76. Copyright 2020 Wiley-VCH Verlag GmbH & Co. KGaA, Weinheim. Panels (e and f) are adapted with permission from ref 77. Copyright 2019 American Chemical Society.

the amorphous WO_{3-x} film achieved ultrahigh SERS activity compared to the crystalline WO_{3-x} film (Figure 6e), with a detection limit of 10^{-9} M for R6G (Figure 6f), and the EF was calculated to be ≈11.635×10^6 at a R6G concentration of 10^{-5} M.

3.3. Tunable Plasmon Resonance Effect

The excitation of the surface plasmon resonance is also an important factor in realizing the effective enhancement of SERS.[62,63] Compared with traditional noble metal substrates, the relatively weak plasmon resonance of semiconductors severely restricts their practical applications. However, the plasmon resonance effect in visible region can be observed in some amorphous semiconductors based on the advantage of their peculiar structure. For example, amorphous H_xMoO_3 quantum dots with tunable plasmon resonance properties from the visible to the near-infrared light region have been reported.[64] Therefore, the electromagnetic field around the probe molecules adsorbed on the surface was enhanced (Figure 7a). Moreover, these amorphous H_xMoO_3 quantum dots have demonstrated excellent SERS enhancement for methylene blue (MB), Rh6G and rhodamine B (RhB). Especially, the enhancement factor of MB molecules reached up to 9.5×10^5 (Figure 7b, c). Similarly, the amorphization of TiO_2 was found to shift LSPR toward the near-infrared, and the SERS activity was enhanced by stronger electromagnetic enhancement.[65] Combined with the photoinduced charge transfer (PICT) between the substrate and the molecule, this hydrogenated black TiO_2 nanowire could achieve an enhancement factor of up to 1.20×10^6 (Figure 7d). Moreover, this SERS substrate also exhibited good cycling stability, as shown in Figure 7e.

In summary, amorphous materials can enhance the Raman signal of absorbed molecules in several ways, as listed below:

1. The abundant dangling bands and the metastable electronic states expand the active region of electrons on the surface of amorphous materials, while also facilitating the formation of surface complexes with adsorbed molecules, which is conducive to the CT process under photoexcitation.[23,59,60,66]
2. Due to the long-range disorder of amorphous materials, the band tails consisting of localized state electrons exist at the bottom of their conduction band and the top of their valence band, thus reducing the band gap and realizing a tunable energy level to facilitate the CT process.[22,24,61,67,68]
3. Amorphous materials always possess a defect energy level in their forbidden bands, which can be used as an "energy level springboard" during the PICT process.[24,61] This is conducive to the energy level coupling and electron leap between the substrate and the molecules.

4. AMORPHOUS MATERIALS FOR ENHANCED MECHANICAL PROPERTY

Amorphous materials exhibit unique mechanical properties, such as high strength, fracture toughness, and viscoelasticity. For more than half a century, scientists have been studing amorphous materials (especially bulk metallic glasses) with unique properties.[25,26] One of the most significant achievements is the discovery of the size effect of amorphous materials.[69−71] By reducing the size of amorphous materials, the mechanical properties can be further improved. For example, the strength of

https://doi.org/10.1021/jacsau.3c00418
JACS Au 2023, 3, 2660−2676

submicron CuZr-based amorphous alloys can be enhanced from 1.5 GPa (bulk metallic glass) to ∼2.5 GPa, and the elastic limit is increased from ∼2% (bulk metallic glass) to ∼2.5%, while the strength of nanosized CuZr-based amorphous alloys is enhanced to ∼3.5 GPa, and the elastic limit is increased to ∼4%, or even higher.[27] The enhancement could be due to fewer amorphous rheological units in small amorphous alloys. However, it should be noted that most of the current research revolves around metallic glass, while studies on nonmetallic amorphous nanomaterials are still in their infancy. This section reviews the unique mechanical properties of nonmetallic amorphous nanomaterials, crystalline−amorphous dual phase nanomaterials, and their composites.

4.1. Amorphous Nanomaterials and Their Composites

High strength and high elasticity have always been the ultimate goals in materials design. However, the lack of long-range order in the microstructure of amorphous nanomaterials makes it difficult to dynamically study the strength and elastic mechanism of amorphous nanomaterials on the atomic scale. The elastic deformation mechanism of amorphous silica nanowires was investigated by *in situ* elastic stretching experiments using TEM.[72] Radial distribution functions (RDFs) calculated from SAED patterns revealed that the high elastic strain of silica nanowires was mainly due to the elastic elongation of the bond length and the change in bond angle due to the amorphous structure. Amorphous zirconia nanowires were also prepared (Figure 8a) to verify the mechanical properties using an *in situ* mechanical stretching device in a scanning electron microscope (SEM). Figure 8b shows that amorphous zirconia nanowires have not only high elasticity (∼5.6%) but also extremely high tensile strength (2.76 GPa) compared to their crystalline counterparts.[73] It is worth noting that the maximum strain of the amorphous zirconia nanowire could reach 8.1%. In other words, the nanowire underwent plastic deformation of 2.5% when the maximum tensile strain was reached. Meanwhile, the calculation results from the stress−strain curves showed that the modulus of the amorphous zirconia was about 43 GPa, which is much lower than that of the bulk crystalline zirconia (∼220 GPa), showing that by establishing the dynamic mechanical dissipation model of the amorphous structure, a new mechanism of "stress shear dissipation" is proposed. This characteristic indicates that amorphous zirconia nanowires have a certain degree of "viscoelasticity", just like high-molecular polymers. Interestingly, a recent study has revealed that the tensile and compressive properties of amorphous materials are asymmetric at the submicron scale.[74] That is to say, once the brittle material in the conventional sense is transformed into an amorphous subnanomaterial, there is an inverse and unusually apparent tensile strength that greatly exceeds the compressive strength. The authors point out that this is due to the reduction of the shear modulus and the densification of the shear-activated configuration under compression, which change the size of the activation energy barrier for the fundamental shear event. This discovery paves the way for the development of high-performance amorphous nanomaterials. In addition, the highly elastic amorphous hollow and porous N-doped carbon/amorphous MoS_3 nanocages were prepared as electrode materials by a template method.[75] *In-situ* mechanical tests showed that the amorphous MoS_3 nanocages were superplastic and could exhibit large deformation during the loading without breaking, which means that the amorphous nanocages could resist the volume expansion during battery charging and discharging, thus providing higher stability.

Another characteristic of amorphous nanomaterials is high viscoelasticity. To further explore the viscoelastic properties, the damaged enamel was successfully coated with a layer of amorphous zirconia by precisely controlling the nucleation and growth rates of zirconia.[76] It is worth noting that there is a strong chemical bond interaction between the amorphous zirconia layer and the intrinsic enamel, as demonstrated by Fourier transform infrared (FTIR) and Raman spectroscopy, guaranteeing protection of damaged tooth enamel. Nanoindentation was employed to test the enamel before and after the restoration to obtain a damping coefficient (tan δ), which is usually used to study viscoelasticity. The results showed that the damping coefficient of the repaired enamel was even slightly higher than that of the original enamel, indicating that the amorphous coating layer can better withstand external pressure to protect the structure inside the enamel from damage. Generally, the performance of the material is not independent. The nanoindentation results also showed that the modulus and hardness of the damaged enamel decreased from 90.1 and 6.0 GPa of the original intact enamels to 34.5 and 2.6 GPa, respectively. When coated with an amorphous zirconia layer, as shown in Figure 8c, the strength and modulus of the repaired enamel quickly recovered to 82.5 and 5.2 GPa, which were 2.4 times and 2.0 times higher than those of the damaged enamel, respectively (Figure 8d). It is worth noting that the amorphous zirconia also provided a smooth hydrophilic surface, which will effectively resist the adhesion and proliferation of bacteria.

The high viscoelasticity of the amorphous materials makes it suitable for the biological applications. Through optimal selection after a natural evolutionary process, the natural periodontal ligament with a fiber bundle structure can facilitate the energy dissipation under external load, enabling the alveolar bone to withstand extremely high occlusal loads (>300 N). In order to meet the requirements of multiple mechanical properties of the periodontal ligament, a high-strength titanium oxide array ligament was prepared, which not only enhanced the osseointegration ability, but also showed the biomechanical adaptability.[78] The biomimetic array ligament has a fine stiffness comparable to that of natural bone, and it has a strong interfacial bond with the Ti substrate to achieve long-term stability. Due to the excellent viscoelasticity of the amorphous titanium oxide array ligament and the synergistic effect of interfacial slippage, it has an energy dissipation function similar to that of the natural periodontal ligament. Compared with Ti-containing implants, the amorphous titanium oxide array membrane reduced the effective stress transmitted from the implant to the peri-implant bone by approximately 30%.

In addition, the abundant dangling bonds of amorphous nanomaterials also enhance the interfacial connection between crystalline and amorphous surfaces or between different amorphous surfaces by forming interfacial chemical bonds. As a result, some amorphous nanomaterials have attractive self-healing properties. For instance, SiC nanofibers with a diameter of 150 nm could show a high tensile strength of 8.8 GPa during the first tensile test in TEM (Figure 8e), and the nanofibers self-healed after unloading and the tensile strength was still as high as 5.6 GPa in the second tensile cycle (Figure 8f).[77] The strong interfacial interaction resulted from the presence of a large number of dangling bonds, and the opposite charges at the fracture surfaces mainly contributed to the outstanding self-healing performance. Another typical example is the deposition

https://doi.org/10.1021/jacsau.3c00418
JACS Au 2023, 3, 2660−2676

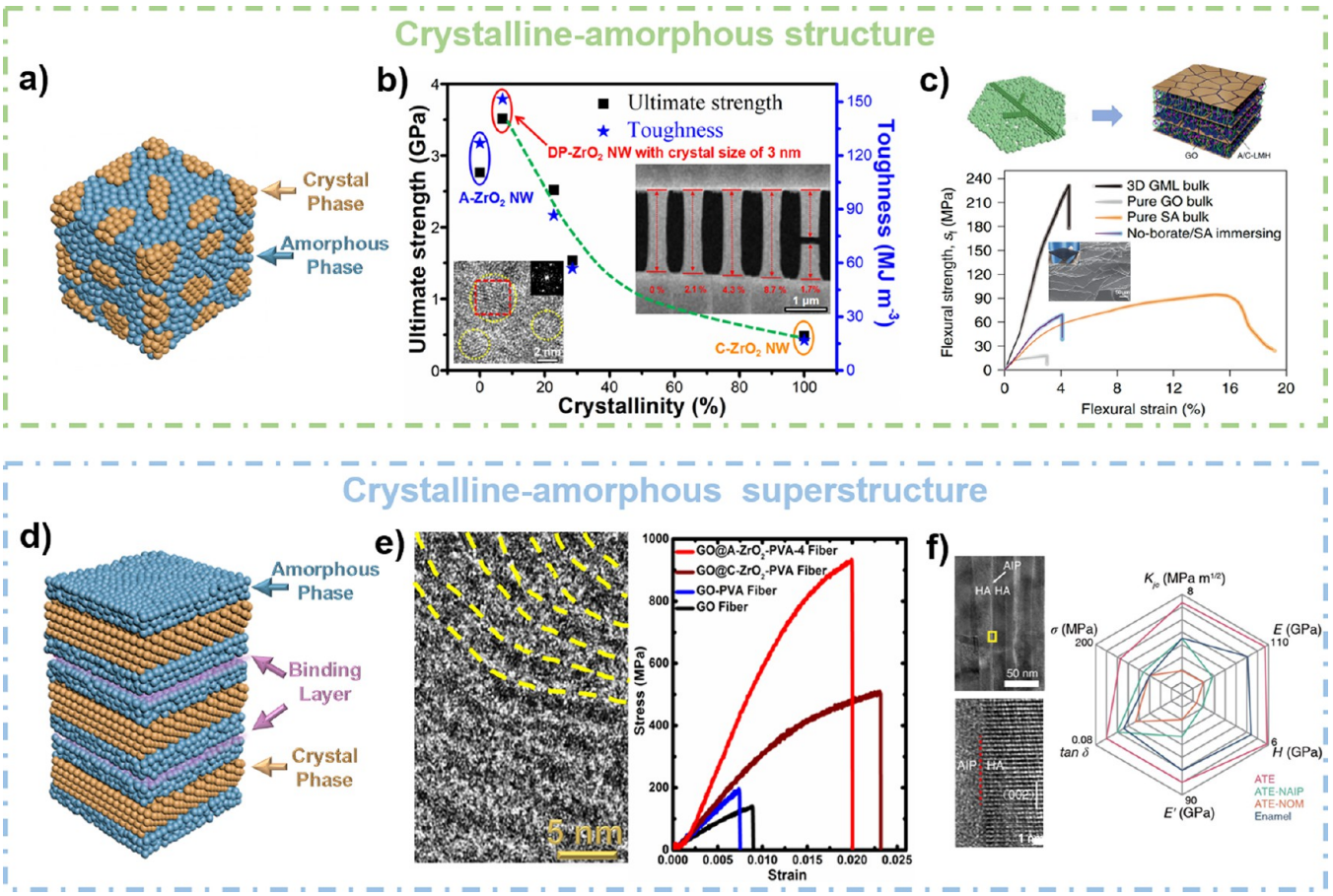

Figure 9. Crystalline−amorphous dual-phase structure. (a) Schematic diagram of the disordered crystalline−amorphous structure. (b) Relationship between the strength/toughness and crystallinity of crystalline−amorphous dual-phase zirconia nanowires. (c) Schematic diagram of the leaf-like crystalline−amorphous nanosheets and their assembled composites (top), the flexural strength-strain curves, the optical photo, and the SEM image of the assembled composites (bottom). (d) Schematic diagram of the crystalline−amorphous superstructure. (e) TEM image of the crystalline−amorphous dual-phase superstructure and the stress−strain curves of the fibers. (f) TEM images show the crystalline−amorphous superstructure of the artificial enamel and the mechanical performance of different enamels. Panels (a), (d), and (e) are adapted with permission from ref 86. Copyright 2022 Elsevier Inc. Panel (b) is adapted with permission from ref 73. Copyright 2019, American Chemical Society. Panel (c) is adapted with permission from ref 87, Copyright 2022 Springer Nature; and ref 88, Copyright 2020 WILEY-VCH Verlag GmbH & Co. KGaA, Weinheim. Panel (f) is adapted with permission from ref 89. Copyright 2022 the American Association for the Advancement of Science.

of amorphous ceramic layers on the surface of the tooth enamel to repair it. The amorphous layer also tends to bind closely to the enamel surface and promote the stability of the coated layer.[76]

After discussing the micromechanics of pure amorphous nanomaterials to describe the intrinsic properties of the amorphous structure, we will further focus on the mechanical properties of their composites at the macroscopic scale to better understand the mechanical properties of amorphous nanomaterials in practical applications. Ultrathin 2D amorphous alumina nanosheets were used as enhanced nanostructure units, and the method of vacuum-assisted suction filtration was adopted to combine them with graphene oxide (GO) and sodium carboxymethyl cellulose.[79] The ternary layered composites were obtained by a controllable layer assembly. The introduction of the alumina nanosheet as a reinforcing phase improved the strength and toughness of the material, which were previously thought to be impossible. By observation of the mechanical behavior, the pull-out mechanism and the mechanical enhancement mechanism of crack deflection were proposed, which could partially explain the strong interfacial interaction. Furthermore, high-strength amorphous alumina was composited with polylactic acid (PLA). Benefiting from the efficient energy dissipation of the amorphous reinforced hybrid interface and the large plastic deformation of the interface at the multilevel scale, the composite possessed a toughness several times higher than that of the original PLA.[80] Similarly, by controlling the nucleation and growth of amorphous zirconia on carbon nanotubes (CNTs), enhanced CNTs were constructed and then successfully assembled with thermoplastic polyurethanes (TPUs) by wet spinning technology.[81] The addition of amorphous zirconia effectively improved the interface and deformation limitation, resulting in amorphous zirconia reinforced fibers with a high strength of 84.6 MPa and high toughness of 126.7 MJ/m^3, superior to those of most reported CNT-TPU fibers.

4.2. Crystalline−Amorphous Dual-Phase Nanomaterials and Their Composites

Although amorphous nanomaterials have high strength, plastic deformation will still occur when the external force applied to amorphous nanomaterials reaches a certain value. The deformation mechanism of amorphous nanomaterials is mainly the shear band, which is the main cause of viscoelasticity, due to the lack of an external environment for dislocation slip. Therefore, the shear band softening effect (the viscoelasticity)

https://doi.org/10.1021/jacsau.3c00418
JACS Au 2023, 3, 2660−2676

limits further improvement of their strength. Interestingly, there are many superstructures with ultrahigh mechanical properties that contain amorphous nanomaterials in nature, such as the elbows of mantis shrimp,[82] nacre,[83,84] enamel,[85] and other biological structures. Further studies have shown that these superstructures are mainly composed of crystalline−amorphous dual phases.

Inspired by the disordered crystalline−amorphous interspersed structure of the mantis shrimp elbow surface, the construction of amorphous−crystalline nanomaterials through structural design would be a wonderful strategy to further improve the mechanical properties of nanomaterials. This idea serves as a favorable way to simultaneously eliminate both the inverse Hall−Petch effect (disadvantages of crystalline nanomaterials) and the shear band softening effect (disadvantages of amorphous nanomaterials). A representative example is the crystalline−amorphous dual-phase zirconia nanowire, which was synthesized by introducing ultrafine zirconia nanocrystals into the amorphous zirconia ceramic matrix by a precise heat treatment (Figure 9a).[73] The *in situ* tensile test in SEM showed that the shear band softening effect and the inverse Hall−Petch effect were successfully suppressed by the controllable combination of amorphous and nanocrystalline structures. Excitingly, the dual-phase zirconia nanowire achieved a simultaneous improvement in strength (3.52 GPa), elastic strain limit (∼7%), and toughness (∼151 MJ·m^{-3}), which is the strongest and toughest zirconia ceramic material reported (Figure 9b). Although the dual-phase structural design has only been implemented in the fabrication of one-dimensional (1D) nanomaterials, it is considered to be a universal strategy applicable to the fabrication of other brittle ceramic materials, as well. Similarly, by utilizing the unsaturated coordination properties at the surface of amorphous nanomaterials, 3D amorphous/crystalline heterogeneous interface construction has been realized. This strategy breaks through the bottleneck of layered dense GO-based composites, which are difficult to prepare in large sizes, and develops a centimeter-sized crystalline−amorphous MnO_2-based GO layered bulk material (Figure 9c).[87] As expected, the as-synthesized product with an amorphous−crystalline structure showed simultaneously high strength, toughness, and impact resistance, surpassing most of the GO-based bulk composite plates reported to date at the centimeter scale. Wu et al. utilized magnetron sputtering to create a disordered crystalline−amorphous alloy material[90] and thermodynamic control to construct a nanoscale crystalline−amorphous layer-by-layer structure.[91] These materials possessed a dual-phase structure and displayed exceptional mechanical properties, demonstrating the effectiveness of the crystalline−amorphous strengthening strategy.

Some biomineralized hard tissues (e.g., nacre, enamel, bone, etc.) have satisfactory mechanical properties such as high strength, high modulus, high hardness, and high toughness. In previous studies, an amorphous ordered structure (Figure 9d) has captured the attention of scientists because of its abundant unsaturated dangling bonds, which can effectively improve the adhesion and interaction between the inorganic crystal and organic phases of organisms. Inspired by it, a crystalline−amorphous superstructure was constructed by uniformly growing amorphous zirconia *in situ* on the surface of GO.[86] The GO-based fiber, prepared by wet spinning technology, exhibited high strength (935 MPa) and high toughness (10.6 MJ m^{-3}) (Figure 9e). The excellent mechanical properties are due to the unique amorphous−crystalline superstructure and the strong interfacial interaction created by the abundant unsaturated dangling bonds of the amorphous compound. An attractive feature of this crystalline−amorphous dual-phase superstructure enhancement strategy is that only ordinary GO is required, rather than large-sized GO or reduced graphene oxide (RGO). This is particularly energy-saving as large-sized GO or RGO are usually associated with high energy consumption of raw materials. Importantly, the economically and environment-friendly produced fiber also showed outstanding structural flexibility and could therefore be easily woven into various fabric patterns, offering a promising future for the widespread applications in the next-generation wearable systems.

As the hardest and strongest tissue in the human body, tooth enamel has excellent viscoelasticity and toughness to resist vibration and impact during chewing. It also combines high hardness, high elasticity, high strength, high toughness, and other mechanical properties. Further research also found that there is an inorganic amorphous interstitial layer between the hydroxyapatite nanowires, and this multilevel micro-nanostructure plays a key role in the excellent mechanical properties of tooth enamel. The imitation of artificial tooth enamel has also been successfully achieved from the atomic scale to the macroscopic scale by coating amorphous zirconia on crystalline hydroxyapatite, followed by the ordered assembly of crystalline−amorphous nanorods.[89] The abundant unsaturated bonds of the amorphous components enhance the interfacial interaction with the adjacent crystalline component, which not only solves the difficult problem of "strength-toughness" and "rigidity-elasticity" of traditional materials but also realizes excellent mechanical properties, such as high stiffness (105 GPa), high hardness (5.9 GPa), high viscoelasticity (VFOM, 5.5 GPa), high strength (143 MPa), and high toughness (7.4 MPa m$^{1/2}$) (Figure 9f). The biomimetic enamel material is the closest structure and performance to natural enamel to date, surpassing previously reported enamel-like composites. FTIR, Raman, X-ray photoelectron spectroscopy (XPS) and other characterizations also proved that the amorphous materials formed a strong chemical interaction with the surrounding microstructure. This groundbreaking work speaks volumes about the important role of amorphous materials in improving material properties.

In summary, amorphous materials possess distinct mechanical properties due to their long-range disorder compared with crystalline materials. Additionally, the unsaturated dangling bonds on their surfaces allow effective chemical interactions with their surroundings, making them suitable for composite material applications. The following are the most notable mechanical features of amorphous materials:

1. Amorphous materials exhibit high strength because they lack the dislocations and grain boundaries found in crystals.[73] Their strength is even comparable to the theoretical value of typical materials.[92]

2. Despite the long-range disorder in their atomic arrangement, research has shown that many amorphous materials are not homogeneous and contain shear deformation zones that provide high viscoelasticity.[76,89]

3. The amorphous surface exposes abundant unsaturated dangling bonds, making it more chemically active. Therefore, it is easier to recombine them with other surrounding materials, forming a new superstrong interfacial interaction.[77]

https://doi.org/10.1021/jacsau.3c00418
JACS Au 2023, 3, 2660−2676

It is worth noting that, in the applications of amorphous nanomaterials, it is usually necessary to compound them with other materials, and the properties of two or three amorphous nanomaterials will act simultaneously in the composite materials. In addition, since enhanced stiffness and viscoelasticity cannot be obtained at the same time, the construction of a crystalline−amorphous dual-phase structure could be a good option where viscoelasticity can be controlled to obtain a higher strength and fracture toughness.

5. CONCLUSION AND PERSPECTIVE

This Perspective summarizes recent advances in the application of amorphous nanomaterials in electrocatalysis, SERS and mechanics. Based on the reported beneficial effects, amorphization provides a facile and efficient strategy to further promote the performance over crystallization. Possible mechanisms have been discussed to better understand why the amorphous structures contribute to the enhanced properties. Despite this promise, the research on amorphous nanomaterials is still in its infancy. In this section, we will elaborate on the following difficulties and some preliminary constructive attempts to envision the opportunities and challenges in this field.

1. **Appropriate structural models for amorphous nanomaterials.** Crystalline materials are composed of periodic unit cells with translational and rotational symmetry, and have the characteristics of long-range ordering properties. The theoretical study of crystals is greatly facilitated by simplified models built from the typical unit cells. In contrast, the study of amorphous nanomaterials is not straightforward because of their long-range disordered atomic structures. In fact, amorphization may not lead to a complete collapse of the structure or to a completely random arrangement over a long-range, but only to atomic deviations and bond distortions. The state-of-the-art techniques such as nanobeam electron diffraction (NBED)[93] and atomic electron tomography (AET)[94] have confirmed the existence of short-range ordered units in amorphous materials. Therefore, appropriate structural models of amorphous nanomaterials are essential to build the theoretical mechanism of the system. Targeting the coordinatively unsaturated structures of amorphous nanomaterials, we have proposed two structural models, namely, the incomplete framework model in which structural atoms are missing, and the cluster model in which surface atoms are missing.[21,31] We believe that these models would go some way toward explaining the static and dynamic structural features and structural evolution of amorphous nanomaterials. At the same time, a more general and applicable structural model is also expected to complement the existing models.
2. **The criterion for assessing amorphous-forming ability.** In 2005, the journal *Science* proposed 125 questions that scientists have not answered, and one of the statements related to amorphous materials is that "Molecules in a glass are arranged much like those in liquids but are more tightly packed."[95] For metallic glass systems, they are disordered solids with "frozen" liquid atoms, which renders rapid cooling an effective approach for producing glasses. The tendency of a liquid to form glass when it cools is called "glass-forming ability," and it is the bottleneck that limits the production and application of amorphous alloys.[96,97] In terms of solution-phase synthesis of amorphous nanomaterials, the disordered structure also originates from high-concentration droplets or polymer-induced transformations of liquid precursors.[14] When and why amorphous nanomaterials are solidified from supersaturated solution is also a mystery. Thus, to clarify the evaluation criterion of "amorphous-forming ability" is a key scientific and technical challenge, and systematic experiments are urgently needed. For example, it has been found that low-dimensional nanomaterials have better amorphous-forming ability, because they have abundant surface atoms, and are much less easily trapped by lattices. In addition, in our work, we proposed that the formation ability of amorphous nanomaterials in solution is positively correlated with the solubility product constant (k_{sp}) between ions, and negatively correlated with the reaction rate (υ).[35] It states that if the k_{sp} between effectively deposited ions is larger, or the solid deposition rate is slower, the formation of amorphous materials would be easier. This conclusion may be contrary to the principles of metallic glass, which is characterized by the fact that the faster liquid metal melt is quenched, the easier it is to form glass. The exploration of more general synthesis methods for amorphous nanomaterials with different elemental compositions will definitely encourage the study of more detailed criteria for assessing the amorphous-forming ability.
3. **Machine learning assisted synthesis of amorphous nanomaterials.** As research on amorphous materials is still in its infancy, both universal synthesis methods and the development of functional materials are essential for continued development. However, whether it is quenching to prepare metallic glasses or solution synthesis of amorphous nanomaterials, the preparation process is quite time-consuming, laborious, and resource-intensive. Fortunately, artificial intelligence and machine learning technologies have developed rapidly over the past decade to tackle complicated issues that traditional approaches cannot, such as highly nonlinear or massively combinatorial processes.[98−100] They may provide a promising way to accelerate the development of efficient protocols for the targeted synthesis of amorphous nanomaterials. We also expect them to have a significant impact on the prediction of new types of amorphous nanomaterials, as well as their synthesis conditions, eventually deepening our understanding toward amorphous nanomaterials.
4. **The space-time correlation of amorphous nanomaterials.** Amorphous materials are considered to be in a metastable state compared to crystalline materials which have a stable structure. Just as the relaxation time is one of the key parameters of metallic glasses, the structural evolution of amorphous nanomaterials during their service life has also been widely reported.[101] Thus, in addition to the dynamic structure changes emerging from spatial correlations, the space-time correlation of the local environment is also vital for amorphous nanomaterials. Due to emerging technologies for rapid and advanced *in situ* detection, the structural changes during operation could be detected in real time. However, in order to separate the intrinsic structural relaxation from structural changes in response to external stimuli, multitechnique cooperations are essential for the joint characterizing of the space-time correlation of amorphous nanomaterials.

https://doi.org/10.1021/jacsau.3c00418
JACS Au 2023, 3, 2660−2676

AUTHOR INFORMATION

Corresponding Authors

Xiuyi Yang − *School of Chemistry, Beijing Advanced Innovation Center for Biomedical Engineering, Key Laboratory of Bio-Inspired Smart Interfacial Science and Technology, Beihang University, Beijing 100191, China*; Email: yangxiuyi@buaa.edu.cn

Lin Guo − *School of Chemistry, Beijing Advanced Innovation Center for Biomedical Engineering, Key Laboratory of Bio-Inspired Smart Interfacial Science and Technology, Beihang University, Beijing 100191, China*; orcid.org/0000-0002-6070-2384; Email: guolin@buaa.edu.cn

Authors

Jianxin Kang − *School of Chemistry, Beijing Advanced Innovation Center for Biomedical Engineering, Key Laboratory of Bio-Inspired Smart Interfacial Science and Technology, Beihang University, Beijing 100191, China*

Fengshi Li − *School of Chemistry, Beijing Advanced Innovation Center for Biomedical Engineering, Key Laboratory of Bio-Inspired Smart Interfacial Science and Technology, Beihang University, Beijing 100191, China; Research Institute for Frontier Science, Beihang University, Beijing 100191, China*; orcid.org/0000-0002-6351-0417

Ziyan Xu − *School of Chemistry, Beijing Advanced Innovation Center for Biomedical Engineering, Key Laboratory of Bio-Inspired Smart Interfacial Science and Technology, Beihang University, Beijing 100191, China*

Xiangyu Chen − *School of Chemistry, Beijing Advanced Innovation Center for Biomedical Engineering, Key Laboratory of Bio-Inspired Smart Interfacial Science and Technology, Beihang University, Beijing 100191, China*

Mingke Sun − *School of Chemistry, Beijing Advanced Innovation Center for Biomedical Engineering, Key Laboratory of Bio-Inspired Smart Interfacial Science and Technology, Beihang University, Beijing 100191, China*

Yanhong Li − *School of Chemistry, Beijing Advanced Innovation Center for Biomedical Engineering, Key Laboratory of Bio-Inspired Smart Interfacial Science and Technology, Beihang University, Beijing 100191, China*

Complete contact information is available at: https://pubs.acs.org/10.1021/jacsau.3c00418

Author Contributions

#J.K., F.L., and Z.X. contributed equally to this work.

Notes

The authors declare no competing financial interest.

Biographies

Xiuyi Yang received his Ph.D. degree from the School of Physics, Engineering and Computer Sciences, University of Hertfordshire (UK) in 2021. He then joined Prof. Lin Guo's group in the School of Chemistry, Beihang University (China) as a postdoctor since 2021. His research interests focus on the characteristics and application of antibacterial amorphous nanomaterials.

Lin Guo is a full professor of the School of Chemistry, Beihang University (China). He received his Ph.D. degree from Beijing University, Institute of Technology (China) in 1997. He was a visiting scholar at the Hong Kong University of Science and Technology (China) in 1999 and worked at Dresden University of Technology (Germany) for two years. His research interests focus on developing new synthetic methods of amorphous nanomaterials and exploring their potential applications.

ACKNOWLEDGMENTS

The work was supported by the National Natural Science Foundation of China (52373221, 52002010, U1910208, 52250119, 52102086), the National Key R&D Program of China (2020YFA0710403).

REFERENCES

(1) Huang, W.; Zhu, J.; Wang, M.; Hu, L.; Tang, Y.; Shu, Y.; Xie, Z.; Zhang, H. Emerging Mono-Elemental Bismuth Nanostructures: Controlled Synthesis and Their Versatile Applications. *Adv. Funct. Mater.* **2021**, *31* (10), 2007584.

(2) Molčanov, K.; Stilinović, V. Chemical Crystallography before X-Ray Diffraction. *Angew. Chem., Int. Ed.* **2014**, *53* (3), 638−652.

(3) Huang, W.; Wang, M.; Hu, L.; Wang, C.; Xie, Z.; Zhang, H. Recent Advances in Semiconducting Monoelemental Selenium Nanostructures for Device Applications. *Adv. Funct. Mater.* **2020**, *30* (42), 2003301.

(4) Thomas, J. M. The Birth of X-Ray Crystallography. *Nature* **2012**, *491* (7423), 186−187.

(5) Zeng, Q.; Sheng, H.; Ding, Y.; Wang, L.; Yang, W.; Jiang, J.-Z.; Mao, W. L.; Mao, H.-K. Long-Range Topological Order in Metallic Glass. *Science* **2011**, *332* (6036), 1404−1406.

(6) Keen, D. A.; Goodwin, A. L. The Crystallography of Correlated Disorder. *Nature* **2015**, *521* (7552), 303−309.

(7) Herzer, G. Modern Soft Magnets: Amorphous and Nanocrystalline Materials. *Acta Mater.* **2013**, *61* (3), 718−734.

(8) Su, Y.; Cui, H.; Li, Q.; Gao, S.; Shang, J. K. Strong Adsorption of Phosphate by Amorphous Zirconium Oxide Nanoparticles. *Water Res.* **2013**, *47* (14), 5018−5026.

(9) Xing, J.; Yan, F.; Zhao, Y.; Chen, S.; Yu, H.; Zhang, Q.; Zeng, R.; Demir, H. V.; Sun, X.; Huan, A.; Xiong, Q. High-Efficiency Light-Emitting Diodes of Organometal Halide Perovskite Amorphous Nanoparticles. *ACS Nano* **2016**, *10* (7), 6623−6630.

(10) Wang, Y.; Li, X.; Huang, Z.; Wang, H.; Chen, Z.; Zhang, J.; Zheng, X.; Deng, Y.; Hu, W. Amorphous Mo-Doped $NiS_{0.5}Se_{0.5}$ Nanosheets@Crystalline $NiS_{0.5}Se_{0.5}$ Nanorods for High Current-Density Electrocatalytic Water Splitting in Neutral Media. *Angew. Chem., Int. Ed.* **2023**, *62* (6), No. e202215256.

(11) McEnaney, J. M.; Crompton, J. C.; Callejas, J. F.; Popczun, E. J.; Biacchi, A. J.; Lewis, N. S.; Schaak, R. E. Amorphous Molybdenum Phosphide Nanoparticles for Electrocatalytic Hydrogen Evolution. *Chem. Mater.* **2014**, *26* (16), 4826−4831.

(12) Liang, J.; Liu, P.; Li, Q.; Li, T.; Yue, L.; Luo, Y.; Liu, Q.; Li, N.; Tang, B.; Alshehri, A. A.; Shakir, I.; Agboola, P. O.; Sun, C.; Sun, X. Amorphous Boron Carbide on Titanium Dioxide Nanobelt Arrays for High-Efficiency Electrocatalytic NO Reduction to NH_3. *Angew. Chem., Int. Ed.* **2022**, *61* (18), No. e202202087.

(13) Yang, N.; Cheng, H.; Liu, X.; Yun, Q.; Chen, Y.; Li, B.; Chen, B.; Zhang, Z.; Chen, X.; Lu, Q.; Huang, J.; Huang, Y.; Zong, Y.; Yang, Y.; Gu, L.; Zhang, H. Amorphous/Crystalline Hetero-Phase Pd Nanosheets: One-Pot Synthesis and Highly Selective Hydrogenation Reaction. *Adv. Mater.* **2018**, *30* (39), 1803234.

(14) Gower, L. B. Biomimetic Model Systems for Investigating the Amorphous Precursor Pathway and Its Role in Biomineralization. *Chem. Rev.* **2008**, *108* (11), 4551−4627.

(15) Chung, S.-Y.; Kim, Y.-M.; Kim, J.-G.; Kim, Y.-J. Multiphase Transformation and Ostwald's Rule of Stages during Crystallization of a Metal Phosphate. *Nat. Phys.* **2009**, *5* (1), 68−73.

(16) Jeon, S.; Heo, T.; Hwang, S.-Y.; Ciston, J.; Bustillo, K. C.; Reed, B. W.; Ham, J.; Kang, S.; Kim, S.; Lim, J.; Lim, K.; Kim, J. S.; Kang, M.-H.; Bloom, R. S.; Hong, S.; Kim, K.; Zettl, A.; Kim, W. Y.; Ercius, P.; Park, J.; Lee, W. C. Reversible Disorder-Order Transitions in Atomic Crystal Nucleation. *Science* **2021**, *371* (6528), 498−503.

(17) Wang, D.; Fernandez-Martinez, A. Order from Disorder. *Science* **2012**, *337* (6096), 812−813.

(18) Liu, J.; Hu, Q.; Wang, Y.; Yang, Z.; Fan, X.; Liu, L.-M.; Guo, L. Achieving Delafossite Analog by in Situ Electrochemical Self-Reconstruction as an Oxygen-Evolving Catalyst. *Proc. Natl. Acad. Sci. U. S. A.* **2020**, *117* (36), 21906−21913.
(19) Liu, J.; Nai, J.; You, T.; An, P.; Zhang, J.; Ma, G.; Niu, X.; Liang, C.; Yang, S.; Guo, L. The Flexibility of an Amorphous Cobalt Hydroxide Nanomaterial Promotes the Electrocatalysis of Oxygen Evolution Reaction. *Small* **2018**, *14* (17), 1703514.
(20) Liu, J.; Ji, Y.; Nai, J.; Niu, X.; Luo, Y.; Guo, L.; Yang, S. Ultrathin Amorphous Cobalt-Vanadium Hydr(Oxy)Oxide Catalysts for the Oxygen Evolution Reaction. *Energy Environ. Sci.* **2018**, *11* (7), 1736−1741.
(21) Kang, J.; Qiu, X.; Hu, Q.; Zhong, J.; Gao, X.; Huang, R.; Wan, C.; Liu, L.-M.; Duan, X.; Guo, L. Valence Oscillation and Dynamic Active Sites in Monolayer NiCo Hydroxides for Water Oxidation. *Nat. Catal.* **2021**, *4* (12), 1050−1058.
(22) Wang, X.; Shi, W.; Wang, S.; Zhao, H.; Lin, J.; Yang, Z.; Chen, M.; Guo, L. Two-Dimensional Amorphous TiO_2 Nanosheets Enabling High-Efficiency Photoinduced Charge Transfer for Excellent SERS Activity. *J. Am. Chem. Soc.* **2019**, *141* (14), 5856−5862.
(23) Li, A.; Lin, J.; Huang, Z.; Wang, X.; Guo, L. Surface-Enhanced Raman Spectroscopy on Amorphous Semiconducting Rhodium Sulfide Microbowl Substrates. *iScience* **2018**, *10* (21), 1−10.
(24) Fan, X.; Li, M.; Hao, Q.; Zhu, M.; Hou, X.; Huang, H.; Ma, L.; Schmidt, O. G.; Qiu, T. High SERS Sensitivity Enabled by Synergistically Enhanced Photoinduced Charge Transfer in Amorphous Nonstoichiometric Semiconducting Films. *Adv. Mater. Interfaces* **2019**, *6* (19), 1901133.
(25) Löffler, J. F. Bulk Metallic Glasses. *Intermetallics* **2003**, *11* (6), 529−540.
(26) Wang, W. H.; Dong, C.; Shek, C. H. Bulk Metallic Glasses. *Mater. Sci. Eng. R Rep.* **2004**, *44* (2−3), 45−89.
(27) Tian, L.; Cheng, Y.-Q.; Shan, Z.-W.; Li, J.; Wang, C.-C.; Han, X.-D.; Sun, J.; Ma, E. Approaching the Ideal Elastic Limit of Metallic Glasses. *Nat. Commun.* **2012**, *3* (1), 609.
(28) Seh, Z. W.; Kibsgaard, J.; Dickens, C. F.; Chorkendorff, I.; Nørskov, J. K.; Jaramillo, T. F. Combining Theory and Experiment in Electrocatalysis: Insights into Materials Design. *Science* **2017**, *355* (6321), No. eaad4998.
(29) Nai, J.; Wang, S.; Bai, Y.; Guo, L. Amorphous $Ni(OH)_2$ Nanoboxes: Fast Fabrication and Enhanced Sensing for Glucose. *Small* **2013**, *9* (18), 3147−3152.
(30) Nai, J.; Tian, Y.; Guan, X.; Guo, L. Pearson's Principle Inspired Generalized Strategy for the Fabrication of Metal Hydroxide and Oxide Nanocages. *J. Am. Chem. Soc.* **2013**, *135* (43), 16082−16091.
(31) Nai, J.; Yin, H.; You, T.; Zheng, L.; Zhang, J.; Wang, P.; Jin, Z.; Tian, Y.; Liu, J.; Tang, Z.; Guo, L. Efficient Electrocatalytic Water Oxidation by Using Amorphous Ni-Co Double Hydroxides Nanocages. *Adv. Energy Mater.* **2015**, *5* (10), 1401880.
(32) Wang, S.; Nai, J.; Yang, S.; Guo, L. Synthesis of Amorphous Ni-Zn Double Hydroxide Nanocages with Excellent Electrocatalytic Activity toward Oxygen Evolution Reaction. *Chemnanomat* **2015**, *1* (5), 324−330.
(33) Cai, Z.; Li, L.; Zhang, Y.; Yang, Z.; Yang, J.; Guo, Y.; Guo, L. Amorphous Nanocages of Cu-Ni-Fe Hydr(Oxy)Oxide Prepared by Photocorrosion For Highly Efficient Oxygen Evolution. *Angew. Chem., Int. Ed.* **2019**, *58* (13), 4189−4194.
(34) Yu, J.; Li, A.; Li, L.; Li, X.; Wang, X.; Guo, L. Morphological and Structural Engineering in Amorphous Cu_2MoS_4 Nanocages for Remarkable Electrocatalytic Hydrogen Evolution. *Sci. China Mater.* **2019**, *62* (9), 1275−1284.
(35) Zhao, H.; Zhu, Y.; Li, F.; Hao, R.; Wang, S.; Guo, L. A Generalized Strategy for the Synthesis of Large-Size Ultrathin Two-Dimensional Metal Oxide Nanosheets. *Angew. Chem., Int. Ed.* **2017**, *56* (30), 8766−8770.
(36) Jia, B.; Hao, R.; Huang, Z.; Hu, P.; Li, L.; Zhang, Y.; Guo, L. Creating Ultrathin Amorphous Metal Hydroxide and Oxide Nanosheet Libraries. *J. Mater. Chem. A* **2019**, *7* (9), 4383−4388.
(37) Jia, B.; Yang, J.; Hao, R.; Li, L.; Guo, L. Confined Synthesis of Ultrathin Amorphous Metal-Oxide Nanosheets. *ACS Mater. Lett.* **2020**, *2* (6), 610−615.
(38) Wu, G.; Zheng, X.; Cui, P.; Jiang, H.; Wang, X.; Qu, Y.; Chen, W.; Lin, Y.; Li, H.; Han, X.; Hu, Y.; Liu, P.; Zhang, Q.; Ge, J.; Yao, Y.; Sun, R.; Wu, Y.; Gu, L.; Hong, X.; Li, Y. A General Synthesis Approach for Amorphous Noble Metal Nanosheets. *Nat. Commun.* **2019**, *10* (1), 4855.
(39) He, Y.; Liu, L.; Zhu, C.; Guo, S.; Golani, P.; Koo, B.; Tang, P.; Zhao, Z.; Xu, M.; Zhu, C.; Yu, P.; Zhou, X.; Gao, C.; Wang, X.; Shi, Z.; Zheng, L.; Yang, J.; Shin, B.; Arbiol, J.; Duan, H.; Du, Y.; Heggen, M.; Dunin-Borkowski, R. E.; Guo, W.; Wang, Q. J.; Zhang, Z.; Liu, Z. Amorphizing Noble Metal Chalcogenide Catalysts at the Single-Layer Limit towards Hydrogen Production. *Nat. Catal.* **2022**, *5* (3), 212−221.
(40) Kang, J.; Xue, Y.; Yang, J.; Hu, Q.; Zhang, Q.; Gu, L.; Selloni, A.; Liu, L.-M.; Guo, L. Realizing Two-Electron Transfer in $Ni(OH)_2$ Nanosheets for Energy Storage. *J. Am. Chem. Soc.* **2022**, *144* (20), 8969−8976.
(41) Liu, J.; Guo, L. In Situ Self-Reconstruction Inducing Amorphous Species: A Key to Electrocatalysis. *Matter* **2021**, *4* (9), 2850−2873.
(42) He, Q.; Sheng, B.; Zhu, K.; Zhou, Y.; Qiao, S.; Wang, Z.; Song, L. Phase Engineering and Synchrotron-Based Study on Two-Dimensional Energy Nanomaterials. *Chem. Rev.* **2023**, *123*, 10750.
(43) Kang, J.; Yang, X.; Hu, Q.; Cai, Z.; Liu, L.-M.; Guo, L. Recent Progress of Amorphous Nanomaterials. *Chem. Rev.* **2023**, *123* (13), 8859−8941.
(44) Jiang, H.; He, Q.; Zhang, Y.; Song, L. Structural Self-Reconstruction of Catalysts in Electrocatalysis. *Acc. Chem. Res.* **2018**, *51* (11), 2968−2977.
(45) Zhang, X.; Luo, Z.; Yu, P.; Cai, Y.; Du, Y.; Wu, D.; Gao, S.; Tan, C.; Li, Z.; Ren, M.; Osipowicz, T.; Chen, S.; Jiang, Z.; Li, J.; Huang, Y.; Yang, J.; Chen, Y.; Ang, C. Y.; Zhao, Y.; Wang, P.; Song, L.; Wu, X.; Liu, Z.; Borgna, A.; Zhang, H. Lithiation-Induced Amorphization of $Pd_3P_2S_8$ for Highly Efficient Hydrogen Evolution. *Nat. Catal.* **2018**, *1* (6), 460−468.
(46) Xie, M.; Yang, L.; Ji, Y.; Wang, Z.; Ren, X.; Liu, Z.; Asiri, A. M.; Xiong, X.; Sun, X. An Amorphous Co-Carbonate-Hydroxide Nanowire Array for Efficient and Durable Oxygen Evolution Reaction in Carbonate Electrolytes. *Nanoscale* **2017**, *9* (43), 16612−16615.
(47) Wang, J.; Huang, B.; Ji, Y.; Sun, M.; Wu, T.; Yin, R.; Zhu, X.; Li, Y.; Shao, Q.; Huang, X. A General Strategy to Glassy M-Te (M = Ru, Rh, Ir) Porous Nanorods for Efficient Electrochemical N_2 Fixation. *Adv. Mater.* **2020**, *32* (11), 1907112.
(48) Yu, Z.; Lv, S.; Yao, Q.; Fang, N.; Xu, Y.; Shao, Q.; Pao, C.-W.; Lee, J.-F.; Li, G.; Yang, L.-M.; Huang, X. Low-Coordinated Pd Site within Amorphous Palladium Selenide for Active, Selective, and Stable H_2O_2 Electrosynthesis. *Adv. Mater.* **2023**, *35* (6), 2208101.
(49) Ge, Y.; Huang, Z.; Ling, C.; Chen, B.; Liu, G.; Zhou, M.; Liu, J.; Zhang, X.; Cheng, H.; Liu, G.; Du, Y.; Sun, C.-J.; Tan, C.; Huang, J.; Yin, P.; Fan, Z.; Chen, Y.; Yang, N.; Zhang, H. Phase-Selective Epitaxial Growth of Heterophase Nanostructures on Unconventional 2H-Pd Nanoparticles. *J. Am. Chem. Soc.* **2020**, *142* (44), 18971−18980.
(50) Kang, J.; Chen, X.; Si, R.; Gao, X.; Zhang, S.; Teobaldi, G.; Selloni, A.; Liu, L.; Guo, L. Activating Bi *p*-Orbitals in Dispersed Clusters of Amorphous BiO_x for Electrocatalytic Nitrogen Reduction. *Angew. Chem., Int. Ed.* **2023**, *62* (15), No. e202217428.
(51) Fleischmann, M.; Hendra, P. J.; McQuillan, A. J. Raman Spectra of Pyridine Adsorbed at a Silver Electrode. *Chem. Phys. Lett.* **1974**, *26* (2), 163−166.
(52) Nie, S.; Emory, S. R. Probing Single Molecules and Single Nanoparticles by Surface-Enhanced Raman Scattering. *Science* **1997**, *275* (5303), 1102−1106.
(53) Lee, H. K.; Lee, Y. H.; Koh, C. S. L.; Phan-Quang, G. C.; Han, X.; Lay, C. L.; Sim, H. Y. F.; Kao, Y.-C.; An, Q.; Ling, X. Y. Designing Surface-Enhanced Raman Scattering (SERS) Platforms beyond Hotspot Engineering: Emerging Opportunities in Analyte Manipulations and Hybrid Materials. *Chem. Soc. Rev.* **2019**, *48* (3), 731−756.

https://doi.org/10.1021/jacsau.3c00418
JACS Au 2023, 3, 2660−2676

(54) Yang, B.; Jin, S.; Guo, S.; Park, Y.; Chen, L.; Zhao, B.; Jung, Y. M. Recent Development of SERS Technology: Semiconductor-Based Study. *ACS Omega* **2019**, *4* (23), 20101−20108.
(55) Filippin, N.; Castillo-Seoane, J.; López-Santos, M. C.; Rojas, C. T.; Ostrikov, K.; Barranco, A.; Sánchez-Valencia, J. R.; Borrás, A. Plasma-Enabled Amorphous TiO_2 Nanotubes as Hydrophobic Support for Molecular Sensing by SERS. *ACS Appl. Mater. Interfaces* **2020**, *12* (45), 50721−50733.
(56) Liu, W.; Xu, Q.; Cui, W.; Zhu, C.; Qi, Y. CO_2-Assisted Fabrication of Two-Dimensional Amorphous Molybdenum Oxide Nanosheets for Enhanced Plasmon Resonances. *Angew. Chem., Int. Ed.* **2017**, *56* (6), 1600−1604.
(57) Ji, W.; Zhao, B.; Ozaki, Y. Semiconductor Materials in Analytical Applications of Surface-Enhanced Raman Scattering: Semiconductor Materials in Analytical Applications. *J. Raman Spectrosc.* **2016**, *47* (1), 51−58.
(58) Yu, J.; Chen, C.; Zhang, Q.; Lin, J.; Yang, X.; Gu, L.; Zhang, H.; Liu, Z.; Wang, Y.; Zhang, S.; Wang, X.; Guo, L. Au Atoms Anchored on Amorphous C_3N_4 for Single-Site Raman Enhancement. *J. Am. Chem. Soc.* **2022**, *144* (48), 21908−21915.
(59) Yu, J.; Chen, C.; Lin, J.; Meng, X.; Qiu, L.; Wang, X. Amorphous $Co(OH)_2$ Nanocages Achieving Efficient Photo-Induced Charge Transfer for Significant SERS Activity. *J. Mater. Chem. C* **2022**, *10* (5), 1632−1637.
(60) Wang, X.; Shi, W.; Jin, Z.; Huang, W.; Lin, J.; Ma, G.; Li, S.; Guo, L. Remarkable SERS Activity Observed from Amorphous ZnO Nanocages. *Angew. Chem., Int. Ed.* **2017**, *56* (33), 9851−9855.
(61) Liu, W.; Wang, Z.; Tang, X.; Liu, Z.; Xiong, Y.; Zhou, X.; Zhu, G.; Zhao, Z.; Yan, W.; Shi, L.; Huang, L.; Liu, Y.; Cui, S.; He, X. Construction of Ultrasensitive Surface-Enhanced Raman Scattering Substates Based on TiO_2 Aerogels. *Adv. Opt. Mater.* **2023**, 2300730.
(62) Hossain, M. K.; Kitahama, Y.; Huang, G. G.; Han, X.; Ozaki, Y. Surface-Enhanced Raman Scattering: Realization of Localized Surface Plasmon Resonance Using Unique Substrates and Methods. *Anal. Bioanal. Chem.* **2009**, *394* (7), 1747−1760.
(63) Willets, K. A.; Van Duyne, R. P. Localized Surface Plasmon Resonance Spectroscopy and Sensing. *Annu. Rev. Phys. Chem.* **2007**, *58*, 267−297.
(64) Li, H.; Xu, Q.; Wang, X.; Liu, W. Ultrasensitive Surface-Enhanced Raman Spectroscopy Detection Based on Amorphous Molybdenum Oxide Quantum Dots. *Small* **2018**, *14* (28), 1801523.
(65) Yang, L.; Peng, Y.; Yang, Y.; Liu, J.; Li, Z.; Ma, Y.; Zhang, Z.; Wei, Y.; Li, S.; Huang, Z.; Long, N. V. Green and Sensitive Flexible Semiconductor SERS Substrates: Hydrogenated Black TiO_2 Nanowires. *ACS Appl. Nano Mater.* **2018**, *1* (9), 4516−4527.
(66) Lin, J.; Zhang, D.; Yu, J.; Pan, T.; Wu, X.; Chen, T.; Gao, C.; Chen, C.; Wang, X.; Wu, A. Amorphous Nitrogen-Doped Carbon Nanocages with Excellent SERS Sensitivity and Stability for Accurate Identification of Tumor Cells. *Anal. Chem.* **2023**, *95* (10), 4671−4681.
(67) Lin, J.; Ren, W.; Li, A.; Yao, C.; Chen, T.; Ma, X.; Wang, X.; Wu, A. Crystal-Amorphous Core-Shell Structure Synergistically Enabling TiO_2 Nanoparticles' Remarkable SERS Sensitivity for Cancer Cell Imaging. *ACS Appl. Mater. Interfaces* **2020**, *12* (4), 4204−4211.
(68) Li, A.; Yu, J.; Lin, J.; Chen, M.; Wang, X.; Guo, L. Increased O 2p State Density Enabling Significant Photoinduced Charge Transfer for Surface-Enhanced Raman Scattering of Amorphous $Zn(OH)_2$. *J. Phys. Chem. Lett.* **2020**, *11* (5), 1859−1866.
(69) Zhao, H.; Li, F.; Wang, S.; Guo, L. Wet Chemical Synthesis of Amorphous Nanomaterials with Well-Defined Morphologies. *Acc. Mater. Res.* **2021**, *2* (9), 804−815.
(70) Yi, J.; Xia, X. X.; Zhao, D. Q.; Pan, M. X.; Bai, H. Y.; Wang, W. H. Micro-and Nanoscale Metallic Glassy Fibers. *Adv. Eng. Mater.* **2010**, *12* (11), 1117−1122.
(71) Deng, Q.; Cheng, Y.; Yue, Y.; Zhang, L.; Zhang, Z.; Han, X.; Ma, E. Uniform Tensile Elongation in Framed Submicron Metallic Glass Specimen in the Limit of Suppressed Shear Banding. *Acta Mater.* **2011**, *59* (17), 6511−6518.
(72) Yue, Y.; Zheng, K.; Zhang, L.; Guo, L. Origin of High Elastic Strain in Amorphous Silica Nanowires. *Sci. China Mater.* **2015**, *58* (4), 274−280.
(73) Li, F.; Zhao, H.; Yue, Y.; Yang, Z.; Zhang, Y.; Guo, L. Dual-Phase Super-Strong and Elastic Ceramic. *ACS Nano* **2019**, *13* (4), 4191−4198.
(74) Wang, Y.; Ding, J.; Fan, Z.; Tian, L.; Li, M.; Lu, H.; Zhang, Y.; Ma, E.; Li, J.; Shan, Z. Tension-Compression Asymmetry in Amorphous Silicon. *Nat. Mater.* **2021**, *20* (10), 1371−1377.
(75) Yu, J.; Xiao, J.; Li, A.; Yang, Z.; Zeng, L.; Zhang, Q.; Zhu, Y.; Guo, L. Enhanced Multiple Anchoring and Catalytic Conversion of Polysulfides by Amorphous MoS_3 Nanoboxes for High-Performance Li-S Batteries. *Angew. Chem., Int. Ed.* **2020**, *59* (31), 13071−13078.
(76) Wei, Y.; Liu, S.; Xiao, Z.; Zhao, H.; Luo, J.; Deng, X.; Guo, L. Enamel Repair with Amorphous Ceramics. *Adv. Mater.* **2020**, *32* (7), 1907067.
(77) Cui, J.; Zhang, Z.; Jiang, H.; Liu, D.; Zou, L.; Guo, X.; Lu, Y.; Parkin, I. P.; Guo, D. Ultrahigh Recovery of Fracture Strength on Mismatched Fractured Amorphous Surfaces of Silicon Carbide. *ACS Nano* **2019**, *13* (7), 7483−7492.
(78) Hou, J.; Xiao, Z.; Liu, Z.; Zhao, H.; Zhu, Y.; Guo, L.; Zhang, Z.; Ritchie, R. O.; Wei, Y.; Deng, X. An Amorphous Peri-Implant Ligament with Combined Osteointegration and Energy-Dissipation. *Adv. Mater.* **2021**, *33* (45), 2103727.
(79) Zhao, H.; Yue, Y.; Zhang, Y.; Li, L.; Guo, L. Ternary Artificial Nacre Reinforced by Ultrathin Amorphous Alumina with Exceptional Mechanical Properties. *Adv. Mater.* **2016**, *28* (10), 2037−2042.
(80) Chen, K.; Ding, J.; Li, L.; Shang, G.; Yue, Y.; Guo, L. Amorphous Alumina Nanosheets/Polylactic Acid Artificial Nacre. *Matter* **2019**, *1* (5), 1385−1398.
(81) Li, Y.; Liu, S.; Zhao, H.; Guo, L. Strong and Tough TPU Fibers with Orientedly Aligned CNTs Reinforced by Amorphous ZrO_2. *Chem. Res. Chin. Univ.* **2022**, *38* (3), 763−768.
(82) Huang, W.; Shishehbor, M.; Guarín-Zapata, N.; Kirchhofer, N. D.; Li, J.; Cruz, L.; Wang, T.; Bhowmick, S.; Stauffer, D.; Manimunda, P.; Bozhilov, K. N.; Caldwell, R.; Zavattieri, P.; Kisailus, D. A Natural Impact-Resistant Bicontinuous Composite Nanoparticle Coating. *Nat. Mater.* **2020**, *19* (11), 1236−1243.
(83) Nassif, N.; Pinna, N.; Gehrke, N.; Antonietti, M.; Jäger, C.; Cölfen, H. Amorphous Layer around Aragonite Platelets in Nacre. *Proc. Natl. Acad. Sci. U. S. A.* **2005**, *102* (36), 12653−12655.
(84) Cantaert, B.; Kuo, D.; Matsumura, S.; Nishimura, T.; Sakamoto, T.; Kato, T. Use of Amorphous Calcium Carbonate for the Design of New Materials. *ChemPlusChem.* **2017**, *82* (1), 107−120.
(85) La Fontaine, A.; Zavgorodniy, A.; Liu, H.; Zheng, R.; Swain, M.; Cairney, J. Atomic-Scale Compositional Mapping Reveals Mg-Rich Amorphous Calcium Phosphate in Human Dental Enamel. *Sci. Adv.* **2016**, *2* (9), No. e1601145.
(86) Li, F.; Zhao, H.; Sun, X.; Yue, Y.; Wang, Z.; Guo, L. Super-Strong Graphene Oxide-Based Fibers Reinforced by a Crystalline-Amorphous Superstructure. *Matter* **2022**, *5* (12), 4437−4449.
(87) Chen, K.; Tang, X.; Jia, B.; Chao, C.; Wei, Y.; Hou, J.; Dong, L.; Deng, X.; Xiao, T.-H.; Goda, K.; Guo, L. Graphene Oxide Bulk Material Reinforced by Heterophase Platelets with Multiscale Interface Crosslinking. *Nat. Mater.* **2022**, *21* (10), 1121−1129.
(88) Jia, B.; Chen, W.; Luo, J.; Yang, Z.; Li, L.; Guo, L. Construction of MnO_2 Artificial Leaf with Atomic Thickness as Highly Stable Battery Anodes. *Adv. Mater.* **2020**, *32* (1), 1906582.
(89) Zhao, H.; Liu, S.; Wei, Y.; Yue, Y.; Gao, M.; Li, Y.; Zeng, X.; Deng, X.; Kotov, N. A.; Guo, L.; Jiang, L. Multiscale Engineered Artificial Tooth Enamel. *Science* **2022**, *375* (6580), 551−556.
(90) Wu, G.; Balachandran, S.; Gault, B.; Xia, W.; Liu, C.; Rao, Z.; Wei, Y.; Liu, S.; Lu, J.; Herbig, M.; Lu, W.; Dehm, G.; Li, Z.; Raabe, D. Crystal-Glass High-Entropy Nanocomposites with Near Theoretical Compressive Strength and Large Deformability. *Adv. Mater.* **2020**, *32* (34), 2002619.
(91) Wu, G.; Liu, C.; Brognara, A.; Ghidelli, M.; Bao, Y.; Liu, S.; Wu, X.; Xia, W.; Zhao, H.; Rao, J.; Ponge, D.; Devulapalli, V.; Lu, W.; Dehm,

https://doi.org/10.1021/jacsau.3c00418
JACS Au 2023, 3, 2660−2676

G.; Raabe, D.; Li, Z. Symbiotic Crystal-Glass Alloys via Dynamic Chemical Partitioning. *Mater. Today* **2021**, *51*, 6−14.
(92) Wu, G.; Chan, K.-C.; Zhu, L.; Sun, L.; Lu, J. Dual-Phase Nanostructuring as a Route to High-Strength Magnesium Alloys. *Nature* **2017**, *545* (7652), 80−83.
(93) Hirata, A.; Guan, P.; Fujita, T.; Hirotsu, Y.; Inoue, A.; Yavari, A. R.; Sakurai, T.; Chen, M. Direct Observation of Local Atomic Order in a Metallic Glass. *Nat. Mater.* **2011**, *10* (1), 28−33.
(94) Yang, Y.; Zhou, J.; Zhu, F.; Yuan, Y.; Chang, D. J.; Kim, D. S.; Pham, M.; Rana, A.; Tian, X.; Yao, Y.; Osher, S. J.; Schmid, A. K.; Hu, L.; Ercius, P.; Miao, J. Determining the Three-Dimensional Atomic Structure of an Amorphous Solid. *Nature* **2021**, *592* (7852), 60−64.
(95) Kennedy, D.; Norman, C. What Don't We Know? *Science* **2005**, *309* (5731), 75−75.
(96) Russo, J.; Romano, F.; Tanaka, H. Glass Forming Ability in Systems with Competing Orderings. *Phys. Rev. X* **2018**, *8* (2), 021040.
(97) Dasgupta, A.; Broderick, S. R.; Mack, C.; Kota, B. U.; Subramanian, R.; Setlur, S.; Govindaraju, V.; Rajan, K. Probabilistic Assessment of Glass Forming Ability Rules for Metallic Glasses Aided by Automated Analysis of Phase Diagrams. *Sci. Rep.* **2019**, *9* (1), 357.
(98) Ryu, B.; Wang, L.; Pu, H.; Chan, M. K. Y.; Chen, J. Understanding, Discovery, and Synthesis of 2D Materials Enabled by Machine Learning. *Chem. Soc. Rev.* **2022**, *51* (6), 1899−1925.
(99) Tao, H.; Wu, T.; Aldeghi, M.; Wu, T. C.; Aspuru-Guzik, A.; Kumacheva, E. Nanoparticle Synthesis Assisted by Machine Learning. *Nat. Rev. Mater.* **2021**, *6* (8), 701−716.
(100) Empel, C.; Koenigs, R. M. Artificial-Intelligence-Driven Organic Synthesis—En Route towards Autonomous Synthesis? *Angew. Chem., Int. Ed.* **2019**, *58* (48), 17114−17116.
(101) Cheng, Y. Q.; Ma, E. Atomic-Level Structure and Structure-Property Relationship in Metallic Glasses. *Prog. Mater. Sci.* **2011**, *56* (4), 379−473.

https://doi.org/10.1021/jacsau.3c00418
JACS Au 2023, 3, 2660−2676